

# A DPG method for shallow shells \*

Thomas Führer<sup>†</sup>      Norbert Heuer<sup>†</sup>      Antti H. Niemi<sup>‡</sup>

## Abstract

We develop and analyze a discontinuous Petrov–Galerkin method with optimal test functions (DPG method) for a shallow shell model of Koiter type. It is based on a uniformly stable ultraweak formulation and thus converges robustly quasi-uniformly. Numerical experiments for various cases, including the Scordelis–Lo cylindrical roof, elliptic and hyperbolic geometries, illustrate its performance. The built-in DPG error estimator gives rise to adaptive mesh refinements that are capable to resolve boundary and interior layers. The membrane locking is dealt with by raising the polynomial degree only of the tangential displacement trace variable.

*AMS Subject Classification:* 74S05, 74K25, 35J35, 65N30, 35J67

## 1 Introduction

The purpose of this paper is to design a quasi-optimal Galerkin scheme for a shallow shell model of Koiter type that is uniformly stable with respect to important parameters like the shell thickness and its curvature. Our scheme has a built-in error estimator comprised of local contributions. It can be used to steer adaptive mesh refinements, to efficiently solve problems with layers and singularities, including point loads.

Our scheme is a DPG method, short for discontinuous Petrov–Galerkin method with optimal test functions. This is a Galerkin framework proposed by Demkowicz and Gopalakrishnan [13, 14, 17]. It aims at an automatic discrete inf-sup stability and usually combines an ultraweak variational formulation [19, 11] and independent trace variables [5] with the use of optimal test functions [2] from product Hilbert spaces. For an early overview and its relation with mixed formulations and the minimum residual method, see [15].

Recently we have exploited the flexibility of the DPG framework to design quasi-optimal Galerkin schemes for the Kirchhoff–Love plate bending model, including the case of non-convex polygonal plates [24, 22, 21]. In this paper we extend the ultraweak variational formulation and

---

\*Supported by ANID-Chile through FONDECYT projects 1190009, 1210391, Ruth och Nils-Erik Stenbäcksstiftelse and Oulun rakennustekniikan säätiö

<sup>†</sup>Facultad de Matemáticas, Pontificia Universidad Católica de Chile, Avenida Vicuña Mackenna 4860, Santiago, Chile, email: {tofuhrrer,nheuer}@mat.uc.cl

<sup>‡</sup>Civil Engineering Research Unit, Faculty of Technology, University of Oulu, Erkki Koiso-Kanttilan katu 5, 90570 Oulu, Finland, email: antti.niemi@oulu.fi

the DPG method developed in [24] to a shallow shell model of Koiter type which has its roots in the vast literature on shell theory. The shallow shell model has been formulated rather concisely in the celebrated textbook by Flügge [20]. It was revived by Pitkäranta *et al.* in [43] where also a Naghdi type variant with non vanishing transverse shear deformations was studied. For more information on the underlying shell theory, we refer the reader to Piila who, also together with Pitkäranta, provided asymptotic analyses for different geometries [36, 37, 38, 39, 40], see also [42, 45]. More recently, numerical analysis for the general Koiter model has been provided in [3, 4, 30, 44, 47].

Restricting the discussion to shells which deviate only slightly from flat plates substantially reduces the technical difficulties of the general shell theory. At the same time, the shallow shell model allows treatment of various relevant engineering problems featuring different shell geometries (parabolic, elliptic, hyperbolic) and preserves the main characteristics of shell mechanics from the numerical analysis point of view. It should also be noted that any smooth shell is shallow in the vicinity of a given point and may be divided into parts that can be analyzed by the shallow shell theory, cf. [29, 32, 33]

A properly designed DPG method combines the advantages of mixed and least squares finite elements by providing direct approximations of both stress and displacement variables as well as a built-in residual for a posteriori error control, see [17, 9]. Our present method features direct approximation of the most important quantities of interest for the shell problem, i.e., normal forces and bending moments together with the middle surface displacements. The evaluation of transverse shear forces and normal rotations still requires post processing. The performance and robustness of our method in approximating different shell deformation states is demonstrated in a variety of benchmark problems involving different shell geometries. In particular, the ability of the adaptive algorithm to capture boundary and interior layers together with the associated stress concentrations is demonstrated. The problem of membrane locking is dealt with by utilizing a higher degree of approximation for the variable that represents the trace of the tangential displacements. As expected, the problem is most severe for pure bending deformations with vanishing membrane strains but it is present in a milder form for any deformation producing bending energy like the edge effects, see, e.g., [41, 12, 43, 31].

Let us comment on some mathematical aspects of our approach for the shallow shell model. Central point for the analysis of ultraweak formulations with product test spaces, as used here, is the study of corresponding trace operators and their images. It is critical to find a test norm that “characterizes” the variational formulation, unknown at that stage, in the sense that it ensures uniform stability of the adjoint problem and uniform boundedness of the bilinear form of the variational formulation. There is a certain canonical procedure based on formal adjoint operators and graph norms, cf. [10] and [16, Appendix A]. For singularly perturbed problems, however, the whole setup has to be chosen very carefully, cf. [18] for convection-dominated diffusion, [27] for reaction-dominated diffusion, and [25] for the Reissner–Mindlin plate bending model. In the case of the shallow shell model, key issue is to introduce norms that take model parameters into account, including the shell thickness, its curvature, the size of the domain, and the type and location of boundary conditions. In [23] we have seen that already moderately sized domains may cause a locking phenomenon when test norms ignore the extension of the domain. Let us

note for that matter that we incorporate the size of the domain by the parameter  $D$  and the boundary conditions through the selection of the tensor  $\mathbf{C}_{\text{disp}}$ , cf. (5) below.

In practice, optimal test functions of DPG schemes have to be approximated. Theoretical results carry over to this case once the existence of a Fortin operator is established, cf. [26]. For the terms appearing in our formulation, Fortin operators have been studied in [26, 22]. But at this point it is open how to construct variants for our Koiter model that are uniformly bounded with respect to critical model parameters. We do not consider this problem here.

An overview of the remainder of this paper is as follows. In the next section we introduce the model problem of a shallow Koiter shell, present a scaled formulation and briefly discuss boundary conditions. Section 3 is devoted to the definition and analysis of trace operators and norms. Principal results in this section are Propositions 3 and 4, respectively proving the identity of two trace norms and characterizing the continuity of test functions. However, as noted before, main contribution is the proper selection of spaces and norms. Our ultraweak formulation is presented in Section 4. Furthermore, we claim its uniform stability (Theorem 5), define the DPG approximation scheme and state its uniform quasi-optimal convergence (Theorem 6). Proofs of Theorems 5 and 6 are given in Section 5. In Section 6 we report on various numerical examples that underline the performance of our DPG scheme. We consider shells with different geometries and show that the built-in error estimator generates appropriate mesh refinements. In particular, it detects interior and boundary layers.

Throughout the paper,  $a \lesssim b$  means that  $a \leq cb$  with a generic constant  $c > 0$  that is independent of important parameters: the (scaled) shell thickness  $d$ , the diameter of  $\Omega$  (the parameter domain in  $\mathbb{R}^2$  of the mid-surface), the curvature tensor  $\mathbf{B}$ , and the underlying mesh  $\mathcal{T}$ . Similarly, we use the notation  $a \gtrsim b$ .

## 2 Model problem

Let  $\Omega \subset \mathbb{R}^2$  be a bounded, simply connected Lipschitz domain with boundary  $\Gamma = \partial\Omega$ . For a vertical load  $f$  and a tangential load  $\mathbf{p}$  we consider

$$\mathbf{B} : \mathbf{N} - \text{div } \text{div } \mathbf{M} = f, \quad \mathbf{M} - \mathcal{C}_b \boldsymbol{\kappa} = 0, \quad \mathbf{N} - \mathcal{C}_m \boldsymbol{\beta} = 0, \quad -\text{div } \mathbf{N} = \mathbf{p} \quad \text{in } \Omega. \quad (1)$$

Here,

$$\boldsymbol{\beta} = \boldsymbol{\varepsilon} \mathbf{u} + \mathbf{B} w, \quad \boldsymbol{\kappa} = -\boldsymbol{\varepsilon} \nabla w, \quad \mathcal{C}_b = \frac{d^3 E}{12} \mathcal{C}, \quad \mathcal{C}_m = d E \mathcal{C},$$

$\boldsymbol{\beta}$  are the membrane strains,  $\mathbf{u} = (u_1, u_2)$  the tangential displacements,  $w$  is the transverse deflection,  $\mathbf{N}$  the membrane forces,  $\boldsymbol{\kappa}$  the bending curvatures,  $\mathbf{M}$  the bending moments, and  $\mathbf{B} = \mathbf{B}^T$  the geometric curvature tensor of the shell mid-surface. The operator  $\boldsymbol{\varepsilon}$  is the symmetric gradient,  $\boldsymbol{\varepsilon} \mathbf{u} := \boldsymbol{\varepsilon}(\mathbf{u}) := \frac{1}{2}(\nabla \mathbf{u} + \nabla \mathbf{u}^T)$ . We assume isotropic, linearly elastic material so that  $\mathcal{C}$  is a positive definite, symmetric fourth-order tensor incorporating the plane stress assumption depending on the Poisson ratio  $\nu$ , whereas we have written the dependence on  $d$  and the Young modulus  $E$  explicitly.

In the following we consider the rescaled displacement  $dE\mathbf{u} \rightarrow \mathbf{u}$  and deflection  $dEw \rightarrow w$ . Then, problem (1) becomes

$$\mathbf{B} : \mathbf{N} - \operatorname{div} \operatorname{div} \mathbf{M} = f \quad \text{in } \Omega, \quad (2a)$$

$$\mathbf{M} + \frac{d^2}{12} \mathcal{C} \varepsilon \nabla w = 0 \quad \text{in } \Omega, \quad (2b)$$

$$\mathbf{N} - \mathcal{C}(\varepsilon \mathbf{u} + \mathbf{B}w) = 0 \quad \text{in } \Omega, \quad (2c)$$

$$-\operatorname{div} \mathbf{N} = \mathbf{p} \quad \text{in } \Omega. \quad (2d)$$

It remains to specify boundary conditions. For ease of presentation we only consider two cases, a simply supported shell,

$$\mathbf{u} = 0, \quad w = 0, \quad \mathbf{n} \cdot \mathbf{M} \mathbf{n} = 0 \quad \text{on } \Gamma \quad (3)$$

and a clamped shell,

$$\mathbf{u} = 0, \quad w = 0, \quad \partial_{\mathbf{n}} w = 0 \quad \text{on } \Gamma. \quad (4)$$

Here,  $\mathbf{n}$  denotes the exterior unit normal vector along  $\Gamma$ , and  $\partial_{\mathbf{n}} w$  is the exterior normal derivative of  $w$ . However, for a piecewise smooth boundary  $\Gamma$ , our theory can be easily extended to mixed cases and any combination of physically meaningful conditions including effective shear forces and point loads. This is due to our mathematical formulation with trace operators that are well defined for polygonal domains (and extend to piecewise smooth boundaries), cf. our setting for Kirchhoff–Love plates [24]. The (natural) condition is that there are sufficient restrictions on the displacement and the deflection to ensure their uniqueness. This enters through the validity of appropriate Poincaré-type inequalities. It is well known that such inequalities do not hold uniformly with respect to the diameter of the underlying physical domain. More importantly, when ignoring such a dependence in the design of minimum residual methods in general, and the DPG method in particular, approximations suffer from locking already for domains of moderate diameter, see [23]. We therefore follow the strategy from [23] which consists in employing scaled norms with parameters that ensure the uniform validity of required Poincaré estimates. In the case of the shallow shell of Koiter type we assume the existence of a symmetric, positive definite tensor  $\mathbf{C}_{\text{disp}}$  of order two and a positive number  $D$  such that

$$D^{-2} \|\mathbf{C}_{\text{disp}} \mathbf{u}\|^2 \lesssim \|\varepsilon \mathbf{u} - \mathbf{B}w\|^2 + d^2 \|\varepsilon \nabla w\|^2, \quad \|w\|^2 \lesssim D^4 \|\varepsilon \nabla w\|^2 \quad (5)$$

hold with generic constants that are independent of  $d$ ,  $\operatorname{diam}(\Omega)$ ,  $\mathbf{B}$ , and the involved functions. In this paper,  $\mathbf{C}_{\text{disp}}$  and  $D$  are constant. But estimates can be easily generalized to  $L_\infty$  tensor/scalar functions  $\mathbf{C}_{\text{disp}}$ ,  $D$  with corresponding uniform properties. In the case of boundary conditions (3) and (4), it is easy to see that

$$D := \operatorname{diam}(\Omega), \quad \mathbf{C}_{\text{disp}} := \operatorname{diag}(c, c) \in \mathbb{R}^{2 \times 2} \quad \text{with} \quad c := \min\left\{1, \frac{d}{D^2 \|\mathbf{B}\|_\infty}\right\}, \quad \min\left\{1, \frac{1}{0}\right\} := 1$$

are possible choices for (5) to hold. However, for a stretched domain,  $D$  can be chosen as the minimum width of  $\Omega$ . In general, the best choice for  $D$  and  $\mathbf{C}_{\text{disp}}$  depends on the boundary

conditions, the shape of  $\Omega$  and the geometric curvature tensor  $\mathbf{B}$ , and in some cases  $\mathbf{C}_{\text{disp}}$  reflects an anisotropy in the stability of the tangential displacements. We refer to Section 6 for specific examples where better (stronger) selections of  $\mathbf{C}_{\text{disp}}$  are possible. For our analysis we need the Poincaré estimate (5) for test functions, cf. (15).

### 3 Trace spaces and norms

In the following we present and study several trace operators, product variants with support on  $\mathcal{S}$  and domain variants with support on  $\Gamma$ . We first recall canonical trace operators related with differential operators of order one. Then, in §3.2, we recall notation and results for operators of second order. Finally, in §3.3, we introduce a combination of trace operators that characterizes traces induced by an ultraweak formulation of problem (2).

Before doing so let us fix some notation. Let  $\mathcal{T}$  be a mesh consisting of general non-intersecting Lipschitz elements  $\{T\}$  so that  $\bar{\Omega} = \cup\{\bar{T}; T \in \mathcal{T}\}$ . We formally denote the mesh skeleton by  $\mathcal{S} = \{\partial T; T \in \mathcal{T}\}$ . For a subdomain  $\omega \subset \Omega$ , generally  $\omega \in \mathcal{T}$  or  $\omega = \Omega$ , we use the standard  $L_2$  spaces  $L_2(\omega)$ ,  $\mathbf{L}_2(\omega) = (L_2(\Omega))^2$  and  $\mathbb{L}_2(\omega) = (L_2(\Omega))^{2 \times 2}$  of scalar, vector and tensor fields of order 2, respectively, with generic norm  $\|\cdot\|_\omega$  and duality  $(\cdot, \cdot)_\omega$ . We drop the index  $\omega$  when  $\omega = \Omega$ . Furthermore,  $\mathbf{H}^1(\omega) = (H^1(\omega))^2$  and  $H^2(\omega)$  are the standard Sobolev spaces,  $\mathbf{H}_0^1(\Omega)$  is the space of  $\mathbf{H}^1(\Omega)$ -functions with zero trace on  $\Gamma$ ,  $H_0^2(\Omega)$  is the space of  $H^2(\Omega)$ -functions with zero trace and normal derivative on  $\Gamma$ ,  $\mathbb{L}_2^s(\omega), \mathbb{L}_2^k(\omega) \subset \mathbb{L}_2(\omega)$  are the subspaces of symmetric and skew-symmetric  $L_2$ -tensors, respectively, and

$$\begin{aligned} \mathbb{H}(\mathbf{div}, \omega) &:= \{\mathbf{T} \in \mathbb{L}_2(\omega); \mathbf{div} \mathbf{T} \in \mathbf{L}_2(\omega)\}, & \mathbb{H}^s(\mathbf{div}, \omega) &:= \mathbb{H}(\mathbf{div}, \omega) \cap \mathbb{L}_2^s(\omega), \\ \mathbb{H}(\mathbf{div} \mathbf{div}, \omega) &:= \{\mathbf{S} \in \mathbb{L}_2^s(\omega); \mathbf{div} \mathbf{div} \mathbf{S} \in \mathbf{L}_2(\omega)\}. \end{aligned}$$

We use the corresponding product spaces, denoted in the same way but replacing  $\omega$  with  $\mathcal{T}$ , e.g.,  $H^1(\mathcal{T}) = \Pi_{T \in \mathcal{T}} H^1(T)$ . The  $L_2(\mathcal{T})$ -dualities are denoted by  $(\cdot, \cdot)_\mathcal{T}$ .

#### 3.1 Canonical trace operators

We define operators

$$\text{tr}^{\text{Grad}} : \begin{cases} \mathbf{H}^1(\mathcal{T}) & \rightarrow \mathbb{H}^s(\mathbf{div}, \mathcal{T})', \\ \mathbf{v} & \mapsto \langle \text{tr}^{\text{Grad}}(\mathbf{v}), \mathbf{T} \rangle_\mathcal{S} := (\mathbf{v}, \mathbf{div} \mathbf{T})_\mathcal{T} + (\boldsymbol{\varepsilon} \mathbf{v}, \mathbf{T})_\mathcal{T} \end{cases}$$

and

$$\text{tr}^{\text{Div}} : \begin{cases} \mathbb{H}(\mathbf{div}, \mathcal{T}) & \rightarrow \mathbf{H}^1(\mathcal{T})' \\ \mathbf{T} & \mapsto \langle \text{tr}^{\text{Div}}(\mathbf{T}), \mathbf{v} \rangle_\mathcal{S} := (\mathbf{T}, \nabla \mathbf{v})_\mathcal{T} + (\mathbf{div} \mathbf{T}, \mathbf{v})_\mathcal{T}. \end{cases}$$

Below, we will systematically use that  $(\nabla \mathbf{v}, \mathbf{T})_\omega = (\boldsymbol{\varepsilon} \mathbf{v}, \mathbf{T})_\omega$  for  $\mathbf{v} \in \mathbf{H}^1(\omega)$ ,  $\mathbf{T} \in \mathbb{L}_2^s(\omega)$ ,  $\omega \subset \Omega$ . That is,

$$\langle \text{tr}^{\text{Grad}}(\mathbf{v}), \mathbf{T} \rangle_\mathcal{S} = \langle \text{tr}^{\text{Div}}(\mathbf{T}), \mathbf{v} \rangle_\mathcal{S} \quad (\mathbf{v} \in \mathbf{H}^1(\mathcal{T}), \mathbf{T} \in \mathbb{H}^s(\mathbf{div}, \mathcal{T})).$$

Analogously we define the canonical trace operators for  $\Omega$  (instead of  $\mathcal{T}$ ) with support on  $\Gamma$ ,  $\text{tr}_\Omega^{\text{Grad}} : \mathbf{H}^1(\Omega) \rightarrow \mathbb{H}^s(\mathbf{div}, \Omega)'$  and  $\text{tr}_\Omega^{\text{Div}} : \mathbb{H}(\mathbf{div}, \Omega) \rightarrow \mathbf{H}^1(\Omega)'$ .

**Proposition 1.** (i) If  $\mathbf{v} \in \mathbf{H}^1(\mathcal{T})$ , then

$$\mathbf{v} \in \mathbf{H}_0^1(\Omega) \iff \langle \text{tr}^{\text{Div}}(\mathbf{T}), \mathbf{v} \rangle_{\mathcal{S}} = 0 \quad \forall \mathbf{T} \in \mathbb{H}(\mathbf{div}, \Omega).$$

(ii) If  $\mathbf{T} \in \mathbb{H}^s(\mathbf{div}, \mathcal{T})$ , then

$$\mathbf{T} \in \mathbb{H}^s(\mathbf{div}, \Omega) \iff \langle \text{tr}^{\text{Grad}}(\mathbf{v}), \mathbf{T} \rangle_{\mathcal{S}} = 0 \quad \forall \mathbf{v} \in \mathbf{H}_0^1(\Omega).$$

*Proof.* For the scalar/vector cases of  $H^1(\mathcal{T})$  and  $H(\mathbf{div}, \mathcal{T})$ , the statements are proved in [10, Theorem 2.3, Remark 2.5]. The vector case (i) can be shown analogously, and (ii) has been proved in [6], see the proof of Lemma 4 around (40) there.  $\square$

### 3.2 Trace operators for Kirchhoff–Love plates

Let us recall the following trace operators from [24],

$$\begin{aligned} \text{tr}^{\text{Ggrad}} : \begin{cases} H^2(\mathcal{T}) & \rightarrow \mathbb{H}(\mathbf{div} \mathbf{div}, \mathcal{T})', \\ z & \mapsto \langle \text{tr}^{\text{Ggrad}}(z), \mathbf{S} \rangle_{\mathcal{S}} := (z, \mathbf{div} \mathbf{div} \mathbf{S})_{\mathcal{T}} - (\varepsilon \nabla z, \mathbf{S})_{\mathcal{T}}, \end{cases} \\ \text{tr}^{\text{dDiv}} : \begin{cases} \mathbb{H}(\mathbf{div} \mathbf{div}, \mathcal{T}) & \rightarrow H^2(\mathcal{T})', \\ \mathbf{S} & \mapsto \langle \text{tr}^{\text{dDiv}}(\mathbf{S}), z \rangle_{\mathcal{S}} := \langle \text{tr}^{\text{Ggrad}}(z), \mathbf{S} \rangle_{\mathcal{S}}. \end{cases} \end{aligned}$$

Again, we also need the trace operators  $\text{tr}_\Omega^{\text{Ggrad}} : H^2(\Omega) \rightarrow \mathbb{H}(\mathbf{div} \mathbf{div}, \Omega)'$  and  $\text{tr}_\Omega^{\text{dDiv}} : \mathbb{H}(\mathbf{div} \mathbf{div}, \Omega) \rightarrow H^2(\Omega)'$ . They are defined as before, only replacing  $\mathcal{T}$  with  $\Omega$ . To deal with the simply supported case (3) we introduce

$$\mathbb{H}_0(\mathbf{div} \mathbf{div}, \Omega) := \{ \mathbf{M} \in \mathbb{H}(\mathbf{div} \mathbf{div}, \Omega); \langle \text{tr}_\Omega^{\text{dDiv}}(\mathbf{M}), z \rangle_{\Gamma} = 0 \quad \forall z \in H^2(\Omega) \cap H_0^1(\Omega) \}.$$

The following relations hold true.

**Proposition 2.** (i) If  $z \in H^2(\mathcal{T})$ , then

$$z \in H_0^2(\Omega) \iff \langle \text{tr}^{\text{dDiv}}(\mathbf{S}), z \rangle_{\mathcal{S}} = 0 \quad \forall \mathbf{S} \in \mathbb{H}(\mathbf{div} \mathbf{div}, \Omega)$$

and

$$z \in H^2(\Omega) \cap H_0^1(\Omega) \iff \langle \text{tr}^{\text{dDiv}}(\mathbf{S}), z \rangle_{\mathcal{S}} = 0 \quad \forall \mathbf{S} \in \mathbb{H}_0(\mathbf{div} \mathbf{div}, \Omega)$$

(ii) If  $\mathbf{S} \in \mathbb{H}(\mathbf{div} \mathbf{div}, \mathcal{T})$ , then

$$\mathbf{S} \in \mathbb{H}(\mathbf{div} \mathbf{div}, \Omega) \iff \langle \text{tr}^{\text{Ggrad}}(z), \mathbf{S} \rangle_{\mathcal{S}} = 0 \quad \forall z \in H_0^2(\Omega)$$

and

$$\mathbf{S} \in \mathbb{H}_0(\mathbf{div} \mathbf{div}, \Omega) \iff \langle \text{tr}^{\text{Ggrad}}(z), \mathbf{S} \rangle_{\mathcal{S}} = 0 \quad \forall z \in H^2(\Omega) \cap H_0^1(\Omega).$$

*Proof.* Statements (i) are proved by [24, Proposition 3.8], [25, Corollary 12], and for statements (ii) we refer to [25, Proposition 11].  $\square$

### 3.3 Shell-specific spaces and trace operators

For  $T \in \mathcal{T}$ , we define the space

$$\mathfrak{V}(T) = \mathbf{H}^1(T) \times H^2(T) \times \mathbb{H}^s(\mathbf{div}, T) \times \mathbb{H}(\mathbf{div} \mathbf{div}, T) \times \mathbb{L}_2^k(T)$$

equipped with the norm (squared)

$$\begin{aligned} \|\mathbf{v}\|_{\mathfrak{V}(T)}^2 := & D^{-2} \|\mathbf{C}_{\text{disp}} \mathbf{v}\|_T^2 + \|\nabla \mathbf{v} - \mathbf{B}z + \mathbf{Q}\|_T^2 + d^2 D^{-4} \|z\|_T^2 + d^2 \|\varepsilon \nabla z\|_T^2 + \|\mathbf{T}\|_T^2 \\ & + D^2 \|\mathbf{C}_{\text{disp}}^{-1} \mathbf{div} \mathbf{T}\|_T^2 + d^{-2} \|\mathbf{S}\|_T^2 + d^{-2} D^4 \|\mathbf{div} \mathbf{div} \mathbf{S} - \mathbf{B} : \mathbf{T}\|_T^2 + c_Q \|\mathbf{Q}\|_T^2 \end{aligned} \quad (6)$$

for  $\mathbf{v} = (\mathbf{v}, z, \mathbf{T}, \mathbf{S}, \mathbf{Q})$ . Here,  $\mathbf{C}_{\text{disp}}$  is a positive definite, symmetric tensor of order two (already announced in (5)) and  $c_Q > 0$  is a constant. Their choice will be made clear when defining the DPG scheme in Section 4, cf. (15) and (18).

Analogously we define  $\mathfrak{V}(\mathcal{T})$  as the product space with respect to  $T \in \mathcal{T}$ , with norm  $\|\cdot\|_{\mathfrak{V}(\mathcal{T})}$  and inner product  $\langle \cdot, \cdot \rangle_{\mathfrak{V}(\mathcal{T})}$ , and the space  $\mathfrak{V}(\Omega)$  with norm  $\|\cdot\|_{\mathfrak{V}(\Omega)}$ , defined like the space  $\mathfrak{V}(T)$  and norm  $\|\cdot\|_{\mathfrak{V}(T)}$  just replacing  $T$  with  $\Omega$ . The  $\mathfrak{V}$ -spaces are used for test functions. For the solution we need the spaces

$$U(T) = \mathbf{H}^1(T) \times H^2(T) \times \mathbb{H}(\mathbf{div}, T) \times \mathbb{H}(\mathbf{div} \mathbf{div}, T) \quad (T \in \mathcal{T})$$

with (squared) norm

$$\begin{aligned} \|(\mathbf{u}, w, \mathbf{N}, \mathbf{M})\|_{U(T)}^2 := & D^{-2} \|\mathbf{C}_{\text{disp}} \mathbf{u}\|_T^2 + \|\varepsilon \mathbf{u} + \mathbf{B}w\|_T^2 + d^2 D^{-4} \|w\|_T^2 + d^2 \|\varepsilon \nabla w\|_T^2 + \|\mathbf{N}\|_T^2 \\ & + c_Q^{-1} \|\text{skew}(\mathbf{N})\|_T^2 + D^2 \|\mathbf{C}_{\text{disp}}^{-1} \mathbf{div} \mathbf{N}\|_T^2 + d^{-2} \|\mathbf{M}\|_T^2 + d^{-2} D^4 \|\mathbf{div} \mathbf{div} \mathbf{M} - \mathbf{B} : \mathbf{N}\|_T^2 \end{aligned} \quad (7)$$

and the corresponding space  $U(\Omega)$  with norm  $\|\cdot\|_{U(\Omega)}$ . Here,  $\text{skew}(\mathbf{N}) := (\mathbf{N} - \mathbf{N}^T)/2$ . Now, to include boundary conditions, we denote by  $U_a(\Omega)$  ( $a \in \{s, c\}$ ) the subspaces of elements  $(\mathbf{u}, w, \mathbf{N}, \mathbf{M}) \in U(\Omega)$  that satisfy (3) ( $a = s$ ) or (4) ( $a = c$ ). The conditions of simple support (3) give the space

$$U_s(\Omega) = \mathbf{H}_0^1(\Omega) \times (H^2(\Omega) \cap H_0^1(\Omega)) \times \mathbb{H}(\mathbf{div}, \Omega) \times \mathbb{H}_0(\mathbf{div} \mathbf{div}, \Omega),$$

cf. [25, Section 3.3], whereas clamped conditions (4) induce

$$U_c(\Omega) = \mathbf{H}_0^1(\Omega) \times H_0^2(\Omega) \times \mathbb{H}(\mathbf{div}, \Omega) \times \mathbb{H}(\mathbf{div} \mathbf{div}, \Omega).$$

We introduce the trace operator (“sK” refers to shallow shell of Koiter type)

$$\text{tr}^{\text{sK}} : \begin{cases} U(\Omega) & \rightarrow \mathfrak{V}(\mathcal{T})', \\ (\mathbf{u}, w, \mathbf{N}, \mathbf{M}) & \mapsto \langle \text{tr}^{\text{sK}}(\mathbf{u}, w, \mathbf{N}, \mathbf{M}), (\mathbf{v}, z, \mathbf{T}, \mathbf{S}, \mathbf{Q}) \rangle_{\mathcal{S}} \end{cases} \quad (8)$$

where  $\langle \text{tr}^{\text{sK}}(\mathbf{u}, w, \mathbf{N}, \mathbf{M}), (\mathbf{v}, z, \mathbf{T}, \mathbf{S}, \mathbf{Q}) \rangle_{\mathcal{S}}$

$$:= \langle \text{tr}^{\text{Grad}}(\mathbf{u}), \mathbf{T} \rangle_{\mathcal{S}} + \langle \text{tr}^{\text{Grad}}(w), \mathbf{S} \rangle_{\mathcal{S}} + \langle \text{tr}^{\text{Div}}(\mathbf{N}), \mathbf{v} \rangle_{\mathcal{S}} - \langle \text{tr}^{\text{dDiv}}(\mathbf{M}), z \rangle_{\mathcal{S}}.$$

It gives rise to the trace spaces

$$\mathbf{H}^{\text{sK}}(\mathcal{S}) := \text{tr}^{\text{sK}}(U(\Omega)), \quad \mathbf{H}_a^{\text{sK}}(\mathcal{S}) := \text{tr}^{\text{sK}}(U_a(\Omega)) \quad (a \in \{s, c\}). \quad (9)$$

A duality between the trace spaces and  $\mathfrak{V}(\mathcal{T})$  is introduced to be consistent with definition (8). That is, for given  $\widehat{\mathbf{u}} \in \mathbf{H}^{\text{sK}}(\mathcal{S})$  and  $\mathbf{v} \in \mathfrak{V}(\mathcal{T})$ , their duality pairing is defined by

$$\langle \widehat{\mathbf{u}}, \mathbf{v} \rangle_{\mathcal{S}} := \langle \text{tr}^{\text{sK}}(\mathbf{u}_0), \mathbf{v} \rangle_{\mathcal{S}}$$

where  $\mathbf{u}_0 \in U(\Omega)$  is such that  $\text{tr}^{\text{sK}}(\mathbf{u}_0) = \widehat{\mathbf{u}}$ .

Of course, the trace spaces have four components consisting of the images of the four trace operators  $\text{tr}^{\text{Grad}}$ ,  $\text{tr}^{\text{Ggrad}}$ ,  $\text{tr}^{\text{Div}}$  and  $\text{tr}^{\text{dDiv}}$ . But just by considering their joint action we achieve robustness of our numerical scheme. To be specific, let us define the norms

$$\begin{aligned} \|\widehat{\mathbf{u}}\|_{\text{sK}, \mathcal{S}} &:= \inf \left\{ \|\mathbf{u}_0\|_{U(\Omega)}; \mathbf{u}_0 \in U(\Omega), \text{tr}^{\text{sK}}(\mathbf{u}_0) = \widehat{\mathbf{u}} \right\}, \\ \|\widehat{\mathbf{u}}\|_{\mathfrak{V}(\mathcal{T})'} &:= \sup_{0 \neq \mathbf{v} \in \mathfrak{V}(\mathcal{T})} \frac{\langle \widehat{\mathbf{u}}, \mathbf{v} \rangle_{\mathcal{S}}}{\|\mathbf{v}\|_{\mathfrak{V}(\mathcal{T})}} \quad \text{for } \widehat{\mathbf{u}} \in \mathbf{H}^{\text{sK}}(\mathcal{S}). \end{aligned}$$

**Proposition 3.** *The identity*

$$\|\widehat{\mathbf{u}}\|_{\mathfrak{V}(\mathcal{T})'} = \|\widehat{\mathbf{u}}\|_{\text{sK}, \mathcal{S}} \quad \forall \widehat{\mathbf{u}} \in \mathbf{H}^{\text{sK}}(\mathcal{S})$$

holds true for  $d > 0$ .

*Proof.* For the bound  $\|\widehat{\mathbf{u}}\|_{\mathfrak{V}(\mathcal{T})'} \leq \|\widehat{\mathbf{u}}\|_{\text{sK}, \mathcal{S}}$  we consider arbitrary elements  $(\mathbf{u}, w, \mathbf{N}, \mathbf{M}) \in U(\Omega)$  and  $(\mathbf{v}, z, \mathbf{T}, \mathbf{S}, \mathbf{Q}) \in \mathfrak{V}(\mathcal{T})$ . Then

$$\begin{aligned} \langle \text{tr}^{\text{sK}}(\mathbf{u}, w, \mathbf{N}, \mathbf{M}), (\mathbf{v}, z, \mathbf{T}, \mathbf{S}, \mathbf{Q}) \rangle_{\mathcal{S}} &= (\mathbf{u}, \text{div } \mathbf{T})_{\mathcal{T}} + (\varepsilon \mathbf{u}, \mathbf{T}) + (w, \text{div } \text{div } \mathbf{S})_{\mathcal{T}} - (\varepsilon \nabla w, \mathbf{S}) \\ &\quad + (\mathbf{N}, \nabla \mathbf{v})_{\mathcal{T}} + (\text{div } \mathbf{N}, \mathbf{v}) + (\mathbf{M}, \varepsilon \nabla z)_{\mathcal{T}} - (\text{div } \text{div } \mathbf{M}, z) \\ &= (\mathbf{u}, \text{div } \mathbf{T})_{\mathcal{T}} + (\varepsilon \mathbf{u} + \mathbf{B}w, \mathbf{T}) + (w, \text{div } \text{div } \mathbf{S} - \mathbf{B} : \mathbf{T})_{\mathcal{T}} + (\mathbf{N}, \nabla \mathbf{v} - \mathbf{B}z + \mathbf{Q})_{\mathcal{T}} \\ &\quad - (\text{div } \text{div } \mathbf{M} - \mathbf{B} : \mathbf{N}, z) + (\text{div } \mathbf{N}, \mathbf{v}) - (\varepsilon \nabla w, \mathbf{S}) + (\mathbf{M}, \varepsilon \nabla z)_{\mathcal{T}} - (\mathbf{N}, \mathbf{Q}) \\ &\leq \|(\mathbf{u}, w, \mathbf{N}, \mathbf{M})\|_{U(\Omega)} \|(\mathbf{v}, z, \mathbf{T}, \mathbf{S}, \mathbf{Q})\|_{\mathfrak{V}(\mathcal{T})} \end{aligned}$$

shows the claimed bound. To prove the other inequality, we formally adapt the technique from [25], see also the abstract framework in [16, Lemma A.10]. Note that, differently to the situation in [25], we are dealing with an operator where all the traces are independent and where different norms are used in the domain of the operator and its dual. Though, as in [25], robust stability requires to combine test functions.

Given  $\widehat{\mathbf{u}} \in \mathbf{H}^{\text{sK}}(\mathcal{S})$ , we first define  $\mathbf{v} = (\mathbf{v}, z, \mathbf{T}, \mathbf{S}, \mathbf{Q}) \in \mathfrak{V}(\mathcal{T})$  as the solution to

$$\langle \mathbf{v}, \delta \mathbf{v} \rangle_{\mathfrak{V}(\mathcal{T})} = \langle \widehat{\mathbf{u}}, \delta \mathbf{v} \rangle_{\mathcal{S}} \quad \forall \delta \mathbf{v} \in \mathfrak{V}(\mathcal{T}) \quad (10)$$

and then  $\mathbf{u}_0 = (\mathbf{u}, w, \mathbf{N}, \mathbf{M}) \in U(\Omega)$  as the solution to

$$\langle \mathbf{u}_0, \delta \mathbf{u} \rangle_{U(\Omega)} = \langle \text{tr}^{\text{sK}}(\delta \mathbf{u}), \mathbf{v} \rangle_{\mathcal{S}} \quad \forall \delta \mathbf{u} \in U(\Omega). \quad (11)$$



Here,  $\langle\langle \cdot, \cdot \rangle\rangle_{U(\Omega)}$  denotes the inner product in  $U(\Omega)$  (the inner product  $\langle\langle \cdot, \cdot \rangle\rangle_{\mathfrak{B}(\mathcal{T})}$  was defined previously). It follows that  $\text{tr}^{\text{sK}}(\mathbf{u}_0) = \widehat{\mathbf{u}}$ , cf. [25, proof of Lemma 4]. Therefore, selecting  $\delta \mathbf{v} = \mathbf{v}$  in (10) and  $\delta \mathbf{u} = \mathbf{u}_0$  in (11), we find that

$$\|\mathbf{v}\|_{\mathfrak{B}(\mathcal{T})}^2 = \langle\widehat{\mathbf{u}}, \mathbf{v}\rangle_{\mathcal{S}} = \|\mathbf{u}_0\|_{U(\Omega)}^2.$$

This proves the inverse inequality,

$$\|\widehat{\mathbf{u}}\|_{\mathfrak{B}(\mathcal{T})'} \geq \frac{\langle\widehat{\mathbf{u}}, \mathbf{v}\rangle_{\mathcal{S}}}{\|\mathbf{v}\|_{\mathfrak{B}(\mathcal{T})}} = \|\mathbf{u}_0\|_{U(\Omega)} \geq \|\widehat{\mathbf{u}}\|_{\text{sK}, \mathcal{S}}.$$

□

It remains to define a global test space with boundary conditions that will serve as the domain of the adjoint problem. To this end we denote by  $\text{tr}_{\Omega}^{\text{sK}} : U(\Omega) \rightarrow \mathfrak{B}(\Omega)'$  the trace operator restricted to continuous test functions,

$$\text{tr}_{\Omega}^{\text{sK}} : \begin{cases} U(\Omega) & \rightarrow \mathfrak{B}(\Omega)', \\ (\mathbf{u}, w, \mathbf{N}, \mathbf{M}) & \mapsto \langle \text{tr}_{\Omega}^{\text{sK}}(\mathbf{u}, w, \mathbf{N}, \mathbf{M}), (\mathbf{v}, z, \mathbf{T}, \mathbf{S}, \mathbf{Q}) \rangle_{\Gamma} \end{cases}$$

with corresponding duality  $\langle \cdot, \cdot \rangle_{\Gamma}$  between  $\text{tr}_{\Omega}^{\text{sK}}(U(\Omega))$  and  $\mathfrak{B}(\Omega)$ . Of course, traces have four components with support on  $\Gamma$ ,

$$\text{tr}_{\Omega}^{\text{sK}}(\mathbf{u}, w, \mathbf{N}, \mathbf{M}) = \left( \text{tr}_{\Omega}^{\text{Grad}}(\mathbf{u}), \text{tr}_{\Omega}^{\text{Ggrad}}(w), \text{tr}_{\Omega}^{\text{Div}}(\mathbf{N}), -\text{tr}_{\Omega}^{\text{dDiv}}(\mathbf{M}) \right). \quad (12)$$

We also need the space  $\mathfrak{B}(\Omega)$  with imposed boundary conditions,

$$\mathfrak{B}_c(\Omega) := \mathbf{H}_0^1(\Omega) \times H_0^2(\Omega) \times \mathbb{H}^s(\mathbf{div}, \Omega) \times \mathbb{H}(\mathbf{div} \mathbf{div}, \Omega) \times \mathbb{L}_2^k(\Omega)$$

and

$$\mathfrak{B}_s(\Omega) := \mathbf{H}_0^1(\Omega) \times (H^2(\Omega) \cap H_0^1(\Omega)) \times \mathbb{H}^s(\mathbf{div}, \Omega) \times \mathbb{H}_0(\mathbf{div} \mathbf{div}, \Omega) \times \mathbb{L}_2^k(\Omega).$$

**Proposition 4.** (i) *The identities*

$$\mathfrak{B}_a(\Omega) = \{ \mathbf{v} \in \mathfrak{B}(\Omega); \langle \text{tr}_{\Omega}^{\text{sK}}(\mathbf{u}_0), \mathbf{v} \rangle_{\Gamma} = 0 \ \forall \mathbf{u}_0 \in U_a(\Omega) \} \quad (a \in \{s, c\})$$

hold true.

(ii) *For  $\mathbf{v} \in \mathfrak{B}(\mathcal{T})$  and  $a \in \{s, c\}$  we have that*

$$\mathbf{v} \in \mathfrak{B}_a(\Omega) \quad \Leftrightarrow \quad \langle \widehat{\mathbf{u}}, \mathbf{v} \rangle_{\mathcal{S}} = 0 \quad \forall \widehat{\mathbf{u}} \in \mathbf{H}_a^{\text{sK}}(\mathcal{S}).$$

*Proof.* Since the trace operators  $\text{tr}^{\text{sK}}$  and  $\text{tr}_{\Omega}^{\text{sK}}$  have independent components as indicated in (12), the kernel relation

$$\langle \text{tr}^{\text{sK}}(\mathbf{u}, w, \mathbf{N}, \mathbf{M}), \mathbf{v} \rangle_{\Gamma} = 0 \quad \forall (\mathbf{u}, w, \mathbf{N}, \mathbf{M}) \in U_a(\Omega)$$

for  $\mathbf{v} = (\mathbf{v}, z, \mathbf{T}, \mathbf{S}, \mathbf{Q}) \in \mathfrak{B}_a(\mathcal{T})$  is equivalent to four separate kernel relations, between  $\mathbf{v}$  and  $\mathbf{N}$ ,  $z$  and  $\mathbf{M}$ ,  $\mathbf{T}$  and  $\mathbf{u}$ ,  $\mathbf{S}$  and  $w$ . Statement (ii) then follows from Propositions 1 and 2, and the first statement is obtained in the same way by simply considering the mesh  $\mathcal{T} = \{\Omega\}$ . □

## 4 Variational formulation and DPG method

We are now in a position to derive an ultraweak variational formulation of problem (2), define our DPG scheme, and state well-posedness of the formulation and robust quasi-optimal approximation properties of the numerical scheme.

To this end we consider problem (2) with general (not necessarily symmetric) tensor  $\mathbf{N}$ , adding the symmetry condition weakly. In this way, normal traces of  $\mathbf{N}$  can be approximated in the standard way. We apply  $12d^{-2}\mathcal{C}^{-1}$  and  $\mathcal{C}^{-1}$  to (2b) and (2c), respectively. Then, testing (2a) with  $-z$ , (2b) with  $\mathbf{S}$ , (2c) with  $\mathbf{T}$ , (2d) with  $\mathbf{v}$ , adding  $(\mathbf{N}, \mathbf{Q}) = 0$  for  $(\mathbf{v}, z, \mathbf{T}, \mathbf{S}, \mathbf{Q}) \in \mathfrak{V}(\mathcal{T})$ , and using the shallow Koiter shell trace operator defined before, we obtain

$$\begin{aligned} & (\mathbf{u}, \operatorname{div} \mathbf{T})_{\mathcal{T}} + (w, \operatorname{div} \operatorname{div} \mathbf{S} - \mathbf{B} : \mathbf{T})_{\mathcal{T}} + (\mathbf{N}, \mathcal{C}^{-1} \mathbf{T} + \nabla \mathbf{v} - \mathbf{B}z + \mathbf{Q})_{\mathcal{T}} \\ & + (\mathbf{M}, 12d^{-2}\mathcal{C}^{-1}\mathbf{S} + \varepsilon \nabla z)_{\mathcal{T}} - \langle \operatorname{tr}^{\text{SK}}(\mathbf{u}, w, \mathbf{N}, \mathbf{M}), (\mathbf{v}, z, \mathbf{T}, \mathbf{S}, \mathbf{Q}) \rangle_{\mathcal{S}} = (\mathbf{p}, \mathbf{v}) - (f, z). \end{aligned}$$

We define the trace as an independent variable with four algebraically independent components,

$$\widehat{\mathbf{u}} = (\widehat{\mathbf{u}}, \widehat{w}, \widehat{\mathbf{N}}_n, \widehat{\mathbf{M}}) := \operatorname{tr}^{\text{SK}}(\mathbf{u}, w, \mathbf{N}, \mathbf{M}),$$

and introduce the spaces

$$\mathfrak{U}_a := \mathbf{L}_2(\Omega) \times L_2(\Omega) \times \mathbb{L}_2(\Omega) \times \mathbb{L}_2^s(\Omega) \times \mathbf{H}_a^{\text{SK}}(\mathcal{S}) \quad (a \in \{s, c\})$$

with norm

$$\|(\mathbf{u}, w, \mathbf{N}, \mathbf{M}, \widehat{\mathbf{u}})\|_{\mathfrak{U}}^2 := D^{-2} \|\mathbf{C}_{\text{disp}} \mathbf{u}\|^2 + d^2 D^{-4} \|w\|^2 + \|\mathbf{N}\|^2 + d^{-2} \|\mathbf{M}\|^2 + \|\widehat{\mathbf{u}}\|_{\text{SK}, \mathcal{S}}^2. \quad (13)$$

Then our variational formulation reads: *Find*  $\mathbf{u} := (\mathbf{u}, w, \mathbf{N}, \mathbf{M}, \widehat{\mathbf{u}}) \in \mathfrak{U}_a$  *such that*

$$b(\mathbf{u}, \mathbf{v}) = L(\mathbf{v}) \quad \forall \mathbf{v} = (\mathbf{v}, z, \mathbf{T}, \mathbf{S}, \mathbf{Q}) \in \mathfrak{V}(\mathcal{T}). \quad (14)$$

Here,

$$\begin{aligned} b(\mathbf{u}, \mathbf{v}) & := (\mathbf{u}, \operatorname{div} \mathbf{T})_{\mathcal{T}} + (w, \operatorname{div} \operatorname{div} \mathbf{S} - \mathbf{B} : \mathbf{T})_{\mathcal{T}} + (\mathbf{N}, \mathcal{C}^{-1} \mathbf{T} + \nabla \mathbf{v} - \mathbf{B}z + \mathbf{Q})_{\mathcal{T}} \\ & + (\mathbf{M}, 12d^{-2}\mathcal{C}^{-1}\mathbf{S} + \varepsilon \nabla z)_{\mathcal{T}} - \langle \widehat{\mathbf{u}}, \mathbf{v} \rangle_{\mathcal{S}} \end{aligned}$$

and

$$L(\mathbf{v}) := (\mathbf{p}, \mathbf{v}) - (f, z).$$

Of course, for the boundary conditions of simple support we select  $a = s$ , and the clamped conditions require  $a = c$ . As mentioned earlier, our theory covers the case of different boundary conditions (not only clamped or simply supported shells). The needed assumption is that the symmetric, positive definite tensor  $\mathbf{C}_{\text{disp}}$  and constant  $D > 0$  be selected so that

$$D^{-2} \|\mathbf{C}_{\text{disp}} \mathbf{v}\|^2 + d^2 D^{-4} \|z\|^2 \lesssim \|\varepsilon \mathbf{v} - \mathbf{B}z\|^2 + d^2 \|\varepsilon \nabla z\|^2 \quad \forall \mathbf{v} = (\mathbf{v}, z, \mathbf{T}, \mathbf{S}, \mathbf{Q}) \in \mathfrak{V}_a(\Omega) \quad (15)$$

holds uniformly with respect to  $d$ ,  $\text{diam}(\Omega)$  and  $\mathbf{B}$ . Of course, in order to control the tangential displacements  $\mathbf{u}$  and transverse deflection  $w$  as strongly as possible, the objective is to select  $\mathbf{C}_{\text{disp}}$  as large as possible (e.g., in terms of its eigenvalues) and  $D > 0$  as small as possible, cf. (13). In the case of a clamped ( $a = c$ ) or simply supported shell ( $a = s$ ), the choices

$$D := \min \text{width}(\Omega), \quad \mathbf{C}_{\text{disp}} := \text{diag}(c, c) \quad \text{with} \quad c := \min\left\{1, \frac{d}{D^2 \|\mathbf{B}\|_\infty}\right\}, \quad \min\left\{1, \frac{1}{0}\right\} := 1 \quad (16)$$

ensure that (15) holds, cf. (5). Here,  $\min \text{width}(\Omega)$  denotes the minimum distance between two parallel lines enclosing  $\Omega$ . For different boundary conditions, giving rise to a space  $U_a(\Omega)$  as the domain of the trace operator  $\text{tr}^{\text{SK}}$ , cf. (9), the space in (15) is

$$\mathfrak{V}_a(\Omega) := \{\mathbf{v} \in \mathfrak{V}(\Omega); \langle \text{tr}_\Omega^{\text{SK}}(\mathbf{u}_0), \mathbf{v} \rangle_\Gamma = 0 \quad \forall \mathbf{u}_0 \in U_a(\Omega)\},$$

cf. Proposition 4. We also need Korn's inequality in the form

$$\|\nabla' \mathbf{v}\|^2 \lesssim \|\varepsilon \mathbf{v}\|^2 \quad \forall \mathbf{v} = (\mathbf{v}, z, \mathbf{T}, \mathbf{S}, \mathbf{Q}) \in \mathfrak{V}_a(\Omega) \quad (17)$$

with skew-symmetric part of the gradient  $\nabla' \mathbf{u} := (\nabla \mathbf{u} - \nabla \mathbf{u}^T)/2$  (usually written as  $\nabla' \mathbf{u} = \frac{1}{2} \text{rot}(\mathbf{u}) \begin{pmatrix} 0 & -1 \\ 1 & 0 \end{pmatrix}$  with  $\text{rot}(\mathbf{u}) := \partial_x u_2 - \partial_y u_1$  for  $\mathbf{u} = (u_1, u_2)^T$ ). It is clear that (17) holds for both boundary conditions,  $a = c$  and  $a = s$ , cf. [7, (11.2.22)]. Furthermore, scaling reveals that the hidden constant does not depend on  $\text{diam}(\Omega)$ . The third parameter to be chosen for the norms is  $c_Q$ , cf. (6), (7). The stability analysis of the adjoint problem in Lemma 8 below suggests to select

$$c_Q := \min\{1, d^2 \|\mathbf{B}\|_\infty^{-2} D^{-4}\}. \quad (18)$$

**Theorem 5.** *For  $d \in (0, 1]$  select  $D$ ,  $\mathbf{C}_{\text{disp}}$  and  $c_Q$  as in (16) and (18), respectively. For given  $f \in L_2(\Omega)$  and  $\mathbf{p} \in \mathbf{L}_2(\Omega)$  there exists a unique solution  $\mathbf{u} = (\mathbf{u}, w, \mathbf{N}, \mathbf{M}, \widehat{\mathbf{u}}) \in \mathfrak{U}_a$  to (14) with boundary conditions (3) ( $a = s$ ) or (4) ( $a = c$ ). It is uniformly bounded,*

$$\|\mathbf{u}\|_{\mathfrak{U}}^2 \lesssim d^{-2} D^4 \|f\|^2 + D^2 \|\mathbf{C}_{\text{disp}}^{-1} \mathbf{p}\|^2$$

*with a hidden constant that is independent of  $f$ ,  $\mathbf{p}$ ,  $\text{diam}(\Omega)$ ,  $\mathbf{B}$ ,  $\mathcal{T}$ , and  $d \in (0, 1]$ . Furthermore,  $(\mathbf{u}, w, \mathbf{N}, \mathbf{M}) \in U_a(\Omega)$  solves (2), and  $\widehat{\mathbf{u}} = \text{tr}^{\text{SK}}(\mathbf{u}, w, \mathbf{N}, \mathbf{M})$ .*

A proof of this theorem is given in §5.1. Now, to define the DPG method, we consider a (family of) discrete subspace(s)  $\mathfrak{U}_{a,h} \subset \mathfrak{U}_a$  (being set on a sequence of meshes  $\mathcal{T}$ ) and introduce the *trial-to-test operator*  $\mathfrak{I} : (\mathfrak{U}_s \cup \mathfrak{U}_c) \rightarrow \mathfrak{V}(\mathcal{T})$  by

$$\langle \mathfrak{I}(\mathbf{u}), \mathbf{v} \rangle_{\mathfrak{V}(\mathcal{T})} = b(\mathbf{u}, \mathbf{v}) \quad \forall \mathbf{v} \in \mathfrak{V}(\mathcal{T}).$$

Then, the DPG method with optimal test functions for problem (2), boundary conditions (3) ( $a = s$ ) or (4) ( $a = c$ ), and based on the variational formulation (14), is: *Find  $\mathbf{u}_h \in \mathfrak{U}_{a,h}$  such that*

$$b(\mathbf{u}_h, \mathfrak{I} \delta \mathbf{u}) = L(\mathfrak{I} \delta \mathbf{u}) \quad \forall \delta \mathbf{u} \in \mathfrak{U}_{a,h}. \quad (19)$$

The following theorem states its robust quasi-optimal best approximation.

**Theorem 6.** For  $d \in (0, 1]$  select  $D$ ,  $\mathbf{C}_{\text{disp}}$  and  $c_Q$  as in (16) and (18), respectively. Let  $f \in L_2(\Omega)$ ,  $\mathbf{p} \in \mathbf{L}_2(\Omega)$  and  $a \in \{s, c\}$  be given. For any finite-dimensional subspace  $\mathfrak{U}_{a,h} \subset \mathfrak{U}_a$  there exists a unique solution  $\mathbf{u}_h \in \mathfrak{U}_{a,h}$  to (19). It satisfies the quasi-optimal error estimate

$$\|\mathbf{u} - \mathbf{u}_h\|_{\mathfrak{U}} \lesssim \|\mathbf{u} - \mathbf{w}\|_{\mathfrak{U}} \quad \forall \mathbf{w} \in \mathfrak{U}_{a,h}$$

with a hidden constant that is independent of  $\mathcal{T}$ ,  $\text{diam}(\Omega)$ ,  $\mathbf{B}$ ,  $d \in (0, 1]$ , and  $\mathfrak{U}_{a,h}$ .

A proof of this theorem is given in §5.1.

**Remark 7.** It is obvious that uniform stability provided by Theorem 5 is not needed to ensure quasi-optimal convergence stated in Theorem 6. For instance, by the Sobolev embedding theorem, a point load  $f$  at  $\mathbf{x}_0 \in \Omega$  is well defined as a duality  $(f, z) := z(\mathbf{x}_0)$  for  $z \in H^2(\mathcal{T})$  (selecting the trace of  $z$  from one side only if  $\mathbf{x}_0$  lies on the skeleton), though it is not bounded uniformly with respect to  $\mathcal{T}$ . Therefore, since  $d^2 D^{-4} \|z\|^2 + d^2 \|\varepsilon \nabla z\|_{\mathcal{T}}^2 \leq \|\mathbf{v}\|_{\mathfrak{V}(\mathcal{T})}^2$  for any  $\mathbf{v} = (\mathbf{v}, z, \mathbf{T}, \mathbf{S}, \mathbf{Q}) \in \mathfrak{V}(\mathcal{T})$ , Theorem 6 also applies to data  $f \in H^2(\mathcal{T})'$ , including point loads, see Section 6.4 for an example.

## 5 Inf-sup conditions and proofs of Theorems 5, 6

Let us formulate the adjoint problem to (2) with boundary conditions (3) ( $a = s$ ) or (4) ( $a = c$ ), and data  $g_1 \in L_2(\Omega)$ ,  $\mathbf{G}_2 \in \mathbb{L}_2^s(\Omega)$ ,  $\mathbf{G}_3 \in \mathbb{L}_2(\Omega)$ , and  $\mathbf{g}_4 \in \mathbf{L}_2(\Omega)$ . Find  $(\mathbf{v}, z, \mathbf{T}, \mathbf{S}, \mathbf{Q}) \in \mathfrak{V}_a(\Omega)$  such that

$$-\mathbf{B} : \mathbf{T} + \text{div div } \mathbf{S} = g_1 \quad \text{in } \Omega, \quad (20a)$$

$$12d^{-2} \mathcal{C}^{-1} \mathbf{S} + \varepsilon \nabla z = \mathbf{G}_2 \quad \text{in } \Omega, \quad (20b)$$

$$\mathcal{C}^{-1} \mathbf{T} + \nabla \mathbf{v} - \mathbf{B}z + \mathbf{Q} = \mathbf{G}_3 \quad \text{in } \Omega, \quad (20c)$$

$$\text{div } \mathbf{T} = \mathbf{g}_4 \quad \text{in } \Omega. \quad (20d)$$

It is a fully non-homogeneous version of (2) with transformed data, negative in-plane displacement and Lagrangian multiplier  $\mathbf{Q}$ . We show that this problem is well posed.

**Lemma 8.** There exists a unique solution  $\mathbf{v} = (\mathbf{v}, z, \mathbf{T}, \mathbf{S}, \mathbf{Q}) \in \mathfrak{V}_a(\Omega)$  to (20), and the bound

$$\|\mathbf{v}\|_{\mathfrak{V}(\Omega)}^2 \lesssim d^{-2} D^4 \|g_1\|^2 + d^2 \|\mathbf{G}_2\|^2 + \|\mathbf{G}_3\|^2 + D^2 \|\mathbf{C}_{\text{disp}}^{-1} \mathbf{g}_4\|^2$$

holds with a constant that is independent of  $\text{diam}(\Omega)$ ,  $\mathbf{B}$ ,  $d \in (0, 1]$  and the given data.

*Proof.* Decomposing  $\mathbf{G}_3 = \mathbf{G}_3^s + \mathbf{G}_3^k$  into its symmetric and skew-symmetric parts we use relations (20b) and (20c) to calculate  $\mathbf{S}$  and  $\mathbf{T}$ ,

$$\mathbf{S} = \frac{d^2}{12} \mathcal{C}(\mathbf{G}_2 - \varepsilon \nabla z), \quad \mathbf{T} = \mathcal{C}(\mathbf{G}_3^s - \varepsilon \mathbf{v} + \mathbf{B}z). \quad (21)$$

We then substitute  $\mathbf{S}$  and  $\mathbf{T}$  in (20a), (20d). Testing (20a) and (20d) with  $-\delta z \in H^2(\Omega)$  and  $\delta \mathbf{v} \in \mathbf{H}^1(\Omega)$ , respectively, an application of the trace operators  $\text{tr}_\Omega^{\text{Grad}}$ ,  $\text{tr}_\Omega^{\text{Ggrad}}$  yields the relations

$$\begin{aligned} & (\mathcal{C}(\mathbf{G}_3^s - \varepsilon \mathbf{v} + \mathbf{B}z), \mathbf{B}\delta z) - \frac{d^2}{12} (\mathcal{C}(\mathbf{G}_2 - \varepsilon \nabla z), \varepsilon \nabla \delta z) - \langle \text{tr}_\Omega^{\text{Ggrad}}(\delta z), \mathbf{S} \rangle_\Gamma = -(g_1, \delta z), \\ & -(\mathcal{C}(\mathbf{G}_3^s - \varepsilon \mathbf{v} + \mathbf{B}z), \varepsilon \delta \mathbf{v}) + \langle \text{tr}_\Omega^{\text{Grad}}(\delta \mathbf{v}), \mathbf{T} \rangle_\Gamma = (\mathbf{g}_4, \delta \mathbf{v}). \end{aligned}$$

Adding both equations, we obtain

$$\begin{aligned} & (\mathcal{C}(\varepsilon \mathbf{v} - \mathbf{B}z), \varepsilon \delta \mathbf{v} - \mathbf{B}\delta z) + \frac{d^2}{12} (\mathcal{C}\varepsilon \nabla z, \varepsilon \nabla \delta z) \\ & = -(g_1, \delta z) + \frac{d^2}{12} (\mathcal{C}\mathbf{G}_2, \varepsilon \nabla \delta z) + (\mathcal{C}\mathbf{G}_3^s, \varepsilon \delta \mathbf{v} - \mathbf{B}\delta z) + (\mathbf{g}_4, \delta \mathbf{v}) \end{aligned} \quad (22)$$

if

$$\langle \text{tr}_\Omega^{\text{Ggrad}}(\delta z), \mathbf{S} \rangle_\Gamma = \langle \text{tr}_\Omega^{\text{Grad}}(\delta \mathbf{v}), \mathbf{T} \rangle_\Gamma = 0.$$

By noting that the boundary conditions for (20) are identical to those for (2) by Proposition 4, cf. (3) resp. (4), it follows that assumption (15) holds. Then, since  $\mathcal{C} : \mathbb{L}_2^s(\Omega) \rightarrow \mathbb{L}_2^s(\Omega)$  is a self-adjoint, positive definite isomorphism, we find that the bilinear form from (22) is coercive. There is a unique solution  $(\mathbf{v}, z) \in \mathbf{H}_0^1(\Omega) \times H_0^2(\Omega)$  (clamped case,  $a = c$ ) or  $(\mathbf{v}, z) \in \mathbf{H}_0^1(\Omega) \times (H^2(\Omega) \cap H_0^1(\Omega))$  (simple support,  $a = s$ ) to (22) that satisfies

$$\begin{aligned} \|\varepsilon \mathbf{v} - \mathbf{B}z\|^2 + d^2 \|\varepsilon \nabla z\|^2 & \lesssim \left( d^{-2} D^4 \|g_1\|^2 + d^2 \|\mathbf{G}_2\|^2 + \|\mathbf{G}_3^s\|^2 + D^2 \|\mathbf{C}_{\text{disp}}^{-1} \mathbf{g}_4\|^2 \right)^{1/2} \\ & \left( D^{-2} \|\mathbf{C}_{\text{disp}} \mathbf{v}\|^2 + \|\varepsilon \mathbf{v} - \mathbf{B}z\|^2 + d^2 D^{-4} \|z\|^2 + d^2 \|\varepsilon \nabla z\|^2 \right)^{1/2}. \end{aligned}$$

Now using (15) explicitly, we obtain

$$\begin{aligned} & D^{-2} \|\mathbf{C}_{\text{disp}} \mathbf{v}\|^2 + \|\varepsilon \mathbf{v} - \mathbf{B}z\|^2 + d^2 D^{-4} \|z\|^2 + d^2 \|\varepsilon \nabla z\|^2 \\ & \lesssim d^{-2} D^4 \|g_1\|^2 + d^2 \|\mathbf{G}_2\|^2 + \|\mathbf{G}_3^s\|^2 + D^2 \|\mathbf{C}_{\text{disp}}^{-1} \mathbf{g}_4\|^2. \end{aligned} \quad (23)$$

Recalling that  $\mathbf{S}$  and  $\mathbf{T}$  are given by (21), one sees that  $(\mathbf{v}, z, \mathbf{T}, \mathbf{S}, \mathbf{Q}) \in \mathfrak{X}_a(\Omega)$  with  $\mathbf{Q} := \mathbf{G}_3^k - \nabla' \mathbf{v}$  solves (20), and is unique. We continue to use relations (21) to bound

$$\|\mathbf{T}\|^2 \lesssim \|\mathbf{G}_3^s\|^2 + \|\varepsilon \mathbf{v} - \mathbf{B}z\|^2, \quad (24)$$

$$d^{-2} \|\mathbf{S}\|^2 \lesssim d^2 \|\mathbf{G}_2\|^2 + d^2 \|\varepsilon \nabla z\|^2. \quad (25)$$

The remaining terms are bounded by using (20a),

$$d^{-2} D^4 \|\text{div div } \mathbf{S} - \mathbf{B} : \mathbf{T}\|^2 = d^{-2} D^4 \|g_1\|^2, \quad (26)$$

and (20d),

$$D^2 \|\mathbf{C}_{\text{disp}}^{-1} \text{div } \mathbf{T}\|^2 = D^2 \|\mathbf{C}_{\text{disp}}^{-1} \mathbf{g}_4\|^2. \quad (27)$$

Noting that  $\|\nabla \mathbf{v} - \mathbf{B}z + \mathbf{Q}\|^2 = \|\boldsymbol{\varepsilon} \mathbf{v} - \mathbf{B}z\|^2 + \|\nabla' \mathbf{v} + \mathbf{Q}\|^2$  and  $\nabla' \mathbf{v} + \mathbf{Q} = \mathbf{G}_3^k$ , (23) implies the bound

$$\|\nabla \mathbf{v} - \mathbf{B}z + \mathbf{Q}\|^2 \lesssim d^{-2} D^4 \|g_1\|^2 + d^2 \|\mathbf{G}_2\|^2 + \|\mathbf{G}_3\|^2 + D^2 \|\mathbf{C}_{\text{disp}}^{-1} \mathbf{g}_4\|^2. \quad (28)$$

By Korn's inequality (17),

$$\|\nabla' \mathbf{v}\|^2 \lesssim \|\boldsymbol{\varepsilon} \mathbf{v} - \mathbf{B}z\|^2 + \|\mathbf{B}\|_\infty^2 \|z\|^2,$$

so that relations  $\mathbf{Q} = \mathbf{G}_3^k - \nabla' \mathbf{v}$  and (23) give

$$\begin{aligned} \|\mathbf{Q}\|^2 &\leq 2(\|\nabla' \mathbf{v}\|^2 + \|\mathbf{G}_3^k\|^2) \lesssim \|\boldsymbol{\varepsilon} \mathbf{v} - \mathbf{B}z\|^2 + \|\mathbf{B}\|_\infty^2 \|z\|^2 + \|\mathbf{G}_3^k\|^2 \\ &\lesssim \max\{1, \|\mathbf{B}\|_\infty^2 d^{-2} D^4\} (d^{-2} D^4 \|g_1\|^2 + d^2 \|\mathbf{G}_2\|^2 + \|\mathbf{G}_3\|^2 + D^2 \|\mathbf{C}_{\text{disp}}^{-1} \mathbf{g}_4\|^2). \end{aligned}$$

This yields

$$c_Q \|\mathbf{Q}\|^2 \lesssim d^{-2} D^4 \|g_1\|^2 + d^2 \|\mathbf{G}_2\|^2 + \|\mathbf{G}_3\|^2 + D^2 \|\mathbf{C}_{\text{disp}}^{-1} \mathbf{g}_4\|^2, \quad (29)$$

cf. (18) for the definition of  $c_Q$ . A combination of (23)–(29) proves the claimed stability bound.  $\square$

**Lemma 9.** *For  $a \in \{s, c\}$  and  $d > 0$ , the adjoint operator  $B^* : \mathfrak{V}(\mathcal{T}) \rightarrow \mathfrak{U}'_a$  is injective.*

*Proof.* We assume that  $(\mathbf{v}, z, \mathbf{T}, \mathbf{S}, \mathbf{Q}) \in \mathfrak{V}(\mathcal{T})$  is such that  $b(\boldsymbol{\delta} \mathbf{u}, \delta w, \boldsymbol{\delta} \mathbf{N}, \boldsymbol{\delta} \mathbf{M}, \boldsymbol{\delta} \widehat{\mathbf{u}}; \mathbf{v}, z, \mathbf{T}, \mathbf{S}, \mathbf{Q}) = 0$  for any  $(\boldsymbol{\delta} \mathbf{u}, \delta w, \boldsymbol{\delta} \mathbf{N}, \boldsymbol{\delta} \mathbf{M}, \boldsymbol{\delta} \widehat{\mathbf{u}}) \in \mathfrak{U}_a$ . The selection of arbitrary  $\boldsymbol{\delta} \widehat{\mathbf{u}} \in \mathbf{H}_a^{\text{SK}}(\mathcal{S})$  (and remaining functions zero) yields  $(\mathbf{v}, z, \mathbf{T}, \mathbf{S}, \mathbf{Q}) \in \mathfrak{V}_a(\Omega)$  by Proposition 4. Therefore,  $(\mathbf{v}, z, \mathbf{T}, \mathbf{S}, \mathbf{Q})$  solves

$$\operatorname{div} \mathbf{T} = 0, \quad \operatorname{div} \operatorname{div} \mathbf{S} - \mathbf{B} : \mathbf{T} = 0, \quad \mathcal{C}^{-1} \mathbf{T} + \nabla \mathbf{v} - \mathbf{B}z + \mathbf{Q} = 0, \quad 12d^{-2} \mathcal{C}^{-1} \mathbf{S} + \boldsymbol{\varepsilon} \nabla z = 0$$

in  $\Omega$ . This is problem (20) with homogeneous data. By Lemma 8,  $(\mathbf{v}, z, \mathbf{T}, \mathbf{S}, \mathbf{Q}) = 0$ .  $\square$

## 5.1 Proofs of Theorems 5, 6

Having all the tools at hand, the proofs are straightforward. For the proof of Theorem 5 we check the standard conditions for the bilinear form  $b(\cdot, \cdot)$  and the functional  $L$ .

### 1. Boundedness of the functional.

$$\begin{aligned} L(\mathbf{v}) &= (\mathbf{p}, \mathbf{v}) - (f, z) \\ &\leq (D^2 \|\mathbf{C}_{\text{disp}}^{-1} \mathbf{p}\|^2 + d^{-2} D^4 \|f\|^2)^{1/2} (D^{-2} \|\mathbf{C}_{\text{disp}} \mathbf{v}\|^2 + d^2 D^{-4} \|z\|^2)^{1/2} \\ &\leq (D^2 \|\mathbf{C}_{\text{disp}}^{-1} \mathbf{p}\|^2 + d^{-2} D^4 \|f\|^2)^{1/2} \|\mathbf{v}\|_{\mathfrak{V}(\mathcal{T})}. \end{aligned}$$

**2. Boundedness of the bilinear form.** Taking into account Proposition 3, the bound  $b(\mathbf{u}, \mathbf{v}) \lesssim \|\mathbf{u}\|_{\mathfrak{U}} \|\mathbf{v}\|_{\mathfrak{V}(\mathcal{T})}$  for any  $\mathbf{u} \in \mathfrak{U}_a$  and  $\mathbf{v} \in \mathfrak{V}(\mathcal{T})$  is immediate.

3. **Injectivity.** This is Lemma 9.

4. **Inf-sup condition.** By [10, Theorem 3.3], the inf-sup condition

$$\sup_{0 \neq (\mathbf{v}, z, \mathbf{T}, \mathbf{S}, \mathbf{Q}) \in \mathfrak{W}(\mathcal{T})} \frac{b(\mathbf{u}, w, \mathbf{N}, \mathbf{M}, \widehat{\mathbf{u}}; \mathbf{v}, z, \mathbf{T}, \mathbf{S}, \mathbf{Q})}{\|(\mathbf{v}, z, \mathbf{T}, \mathbf{S}, \mathbf{Q})\|_{\mathfrak{W}(\mathcal{T})}} \gtrsim \|(\mathbf{u}, w, \mathbf{N}, \mathbf{M}, \widehat{\mathbf{u}})\|_{\mathfrak{U}} \quad (30)$$

for any  $(\mathbf{u}, w, \mathbf{N}, \mathbf{M}, \widehat{\mathbf{u}}) \in \mathfrak{U}_a$  ( $a \in \{s, c\}$ ) follows from the inf-sup conditions

$$\sup_{0 \neq (\mathbf{v}, z, \mathbf{T}, \mathbf{S}, \mathbf{Q}) \in \mathfrak{W}(\mathcal{T})} \frac{\langle \widehat{\mathbf{u}}, (\mathbf{v}, z, \mathbf{T}, \mathbf{S}, \mathbf{Q}) \rangle_{\mathcal{S}}}{\|(\mathbf{v}, z, \mathbf{T}, \mathbf{S}, \mathbf{Q})\|_{\mathfrak{W}(\mathcal{T})}} \gtrsim \|\widehat{\mathbf{u}}\|_{\text{sK}, \mathcal{S}} \quad \forall \widehat{\mathbf{q}} \in \mathbf{H}_a^{\text{sK}}(\mathcal{S}) \quad (31)$$

and

$$\begin{aligned} \sup_{0 \neq (\mathbf{v}, z, \mathbf{T}, \mathbf{S}, \mathbf{Q}) \in \mathfrak{W}_a(\Omega)} \frac{b(\mathbf{u}, w, \mathbf{N}, \mathbf{M}, 0; \mathbf{v}, z, \mathbf{T}, \mathbf{S}, \mathbf{Q})}{\|(\mathbf{v}, z, \mathbf{T}, \mathbf{S}, \mathbf{Q})\|_{\mathfrak{W}(\mathcal{T})}} \\ \gtrsim \left( D^{-2} \|\mathbf{C}_{\text{disp}} \mathbf{u}\|^2 + d^2 D^{-4} \|w\|^2 + \|\mathbf{N}\|^2 + d^{-2} \|\mathbf{M}\|^2 \right)^{1/2} \end{aligned} \quad (32)$$

for any  $(\mathbf{u}, w, \mathbf{N}, \mathbf{M}) \in \mathbf{L}_2(\Omega) \times L_2(\Omega) \times \mathbb{L}_2(\Omega) \times \mathbb{L}_2^s(\Omega)$ .

Relation (31) is true (with constant 1) by Proposition 3, and inf-sup condition (32) holds due to Lemma 8: Selecting data

$$(g_1, \mathbf{G}_2, \mathbf{G}_3, g_4) := (d^2 D^{-4} w, d^{-2} \mathbf{M}, \mathbf{N}, D^{-2} \mathbf{C}_{\text{disp}}^2 \mathbf{u})$$

in (20) with solution  $\mathbf{v}^* \in \mathfrak{W}_a(\Omega)$ , we bound

$$\begin{aligned} \sup_{0 \neq \mathbf{v} \in \mathfrak{W}_a(\Omega)} \frac{b(\mathbf{u}, w, \mathbf{N}, \mathbf{M}, 0; \mathbf{v})}{\|\mathbf{v}\|_{\mathfrak{W}(\mathcal{T})}} &\geq \frac{(w, g_1) + (\mathbf{M}, \mathbf{G}_2) + (\mathbf{N}, \mathbf{G}_3) + (\mathbf{u}, g_4)}{\|\mathbf{v}^*\|_{\mathfrak{W}(\mathcal{T})}} \\ &\gtrsim \frac{d^2 D^{-4} \|w\|^2 + d^{-2} \|\mathbf{M}\|^2 + \|\mathbf{N}\|^2 + D^{-2} \|\mathbf{C}_{\text{disp}} \mathbf{u}\|^2}{\left( d^{-2} D^4 \|g_1\|^2 + d^2 \|\mathbf{G}_2\|^2 + \|\mathbf{G}_3\|^2 + D^2 \|\mathbf{C}_{\text{disp}}^{-1} g_4\|^2 \right)^{1/2}} \\ &= \left( d^2 D^{-4} \|w\|^2 + d^{-2} \|\mathbf{M}\|^2 + \|\mathbf{N}\|^2 + D^{-2} \|\mathbf{C}_{\text{disp}} \mathbf{u}\|^2 \right)^{1/2}. \end{aligned}$$

It remains to note that  $(\mathbf{u}, w, \mathbf{N}, \mathbf{M})$  solves (2), satisfies the selected boundary conditions, (3) or (4), and  $\widehat{\mathbf{u}} = \text{tr}^{\text{sK}}(\mathbf{u}, w, \mathbf{N}, \mathbf{M})$ . This finishes the proof of Theorem 5.

Now, to prove Theorem 6, we recall that, by design of the DPG scheme as a minimum residual method,

$$\|B(\mathbf{u} - \mathbf{u}_h)\|_{\mathfrak{W}(\mathcal{T})'} = \min\{\|B(\mathbf{u} - \mathbf{w})\|_{\mathfrak{W}(\mathcal{T})'}; \mathbf{w} \in \mathfrak{U}_{a,h}\}.$$

Here,  $B : \mathfrak{U}_a \rightarrow \mathfrak{W}(\mathcal{T})'$  is the operator induced by the bilinear form  $b(\cdot, \cdot)$ . The result follows by the uniform equivalence of  $\|\cdot\|_{\mathfrak{U}}$  and  $\|B \cdot\|_{\mathfrak{W}(\mathcal{T})'}$ . Indeed,  $\|B \cdot\|_{\mathfrak{W}(\mathcal{T})'} \lesssim \|\cdot\|_{\mathfrak{U}}$  by the uniform boundedness of  $b(\cdot, \cdot)$ , and the inverse estimate is (30).

## 6 Numerical experiments

In this section, we demonstrate the performance of our DPG method in different benchmark tests. In §6.2, we consider the classical Scordelis–Lo cylindrical shell roof which features a somewhat realistic problem setup related to the design of reinforced concrete roofs. As the name suggests, the problem framework was adopted for benchmarking purposes of computer methods by Scordelis and Lo in [46]. Nowadays, such benchmarking is typically restricted to the evaluation of the maximum vertical displacement in a fixed geometry, but there is some ambiguity in the literature regarding the exact target value. This is because the solution of the problem varies slightly depending on the specific characteristics of the assumed shell model. Following the analytic and semi-analytic procedures presented by Flügge and Briassoulis in [20, 8], we have verified the analytic reference solution for the shallow Koiter model used in our study. The problem itself features long-range angular boundary layers emanating from the straight edges of the roof and conventional finite element methods are subject to moderate membrane locking.

As a second test, in §6.3 we consider the Pitkäranta cylinder obstacle course featuring a closed circular cylindrical shell which is loaded by an axially constant but angularly varying self-balancing normal pressure. Pure membrane and bending dominated deformations are obtained by setting the ends of the cylinder fully clamped (§6.3.1) or leaving them free (§6.3.2), respectively, whereas the so-called simple effect becomes activated for simply supported sliding edges (§6.3.3), see [42]. Again, the semi-analytic reference solution has been computed for each case. Conventionally, no locking is expected for the membrane-dominated case, whereas the inextensional bending modes present for free ends give rise to severe membrane locking. The simple edge effect gives also rise to transverse shear locking for Naghdi type shell models. But these are of no concern for our Koiter type model neglecting the transverse shear strains altogether.

As a final test, in §6.4 we analyze the singular stress system of a shallow shell under a normal point load, cf. [35, 34]. The deformation is known to vary depending on the geometric curvature and thickness of the shell in such a way that the “hot spot”, which is present around the load application point for all curved geometries, spreads into characteristic line layers along the generators of parabolic and hyperbolic shells. By assuming doubly periodic boundary conditions, the singularity can be examined by Fourier analysis. The related parametric effects are relatively complex but the line layers may be associated with the usual angular layers in cylindrical shells and with the corresponding generalized edge effect in hyperbolic geometry. For such deformations, a moderate level of membrane locking is again expected.

Before presenting our numerical results, let us comment on the definition of tensor  $\mathbf{C}_{\text{disp}}$  that influences the control of the tangential displacements, cf. (13). It must be chosen so that (continuous) test functions  $\mathbf{v} = (\mathbf{v}, z, \mathbf{T}, \mathbf{S}, \mathbf{Q}) \in \mathfrak{V}_a(\Omega)$  satisfy assumption (15). By duality it is clear that the boundary conditions describing  $\mathfrak{V}_a(\Omega)$  are those of the model problem to be studied. In other words, the boundary conditions imposed on  $\mathbf{v}$  and  $z$  are the ones for the tangential displacements  $\mathbf{u}$  and the vertical deflection  $w$ , respectively. In all the examples of this section, the conditions on  $w$  (and therefore on  $z$ ) are such that  $\|z\| \lesssim \text{diam}(\Omega)^2 \|\varepsilon \nabla z\|$  by a Poincaré–Friedrichs estimate (cf. [7, (5.9.3)]) and scaling. Furthermore, the conditions on the tangential displacements  $\mathbf{u}$  (and therefore on  $\mathbf{v}$ ) are such that rigid body motions in the



plane (rigid shell modes) are eliminated. Therefore,  $\|\mathbf{v}\| \lesssim \text{diam}(\Omega)\|\boldsymbol{\varepsilon}\mathbf{v}\|$  by Korn's inequality (cf. [7, (11.2.22)]) and scaling. Bounding  $\|\boldsymbol{\varepsilon}\mathbf{v}\| \leq \|\boldsymbol{\varepsilon}\mathbf{v} - \mathbf{B}z\| + \|\mathbf{B}\|_\infty\|z\|$ , and selecting  $D$  such that  $D \simeq \text{diam}(\Omega)$ , we conclude that

$$\begin{aligned} D^{-2}\|\mathbf{v}\|^2 &\lesssim \|\boldsymbol{\varepsilon}\mathbf{v} - \mathbf{B}z\|^2 + \|\mathbf{B}\|_\infty^2 D^4 \|\boldsymbol{\varepsilon}\nabla z\|^2 \\ &\leq \max\{1, d^{-2}\|\mathbf{B}\|_\infty^2 D^4\} (\|\boldsymbol{\varepsilon}\mathbf{v} - \mathbf{B}z\|^2 + d^2\|\boldsymbol{\varepsilon}\nabla z\|^2) \quad \forall \mathbf{v} = (\mathbf{v}, z, \mathbf{T}, \mathbf{S}, \mathbf{Q}) \in \mathfrak{V}_a(\Omega) \end{aligned}$$

for the boundary conditions specified in the examples of this section. That is, (15) holds with

$$D \simeq \text{diam}(\Omega), \quad \mathbf{C}_{\text{disp}} = \text{diag}(c, c), \quad c = \min\{1, d\|\mathbf{B}\|_\infty^{-1}D^{-2}\}. \quad (33)$$

This is a generic choice for  $\mathbf{C}_{\text{disp}}$  as mentioned in Section 2 (recall relations (5) ff.) and claimed in (16) (improved for stretched domains). In some cases below, a stronger selection is in order, and possible. We do not study anisotropic domains here but refer to [23] for such an example.

## 6.1 Setup

Before presenting our numerical results, let us specify the discretization setup. We use shape-regular triangular meshes  $\mathcal{T}$  on  $\Omega$  with maximum mesh-size  $h = \max_{T \in \mathcal{T}} \text{diam}(T)$ . In all the examples,  $\Omega$  is a rectangular domain and we use an initial mesh of four triangles. By  $\mathcal{P}^k(\mathcal{T})$  we denote the space of  $\mathcal{T}$ -piecewise polynomials of degree  $\leq k \in \mathbb{N}_0$ , and  $[\mathcal{RT}^0(\mathcal{T})]^2 \subset \mathbb{H}(\mathbf{div}, \Omega)$  is the space of row-wise lowest-order Raviart–Thomas elements. We also need the subspace  $\mathcal{HCT}(\mathcal{T}) \subset H^2(\Omega)$  consisting of the (reduced) HCT elements (the degrees of freedom are associated with the values at vertices and the values of gradients at vertices). For an edge  $E$  let  $\mathcal{P}^0(E)$  be the space of constants on  $E$ . Then

$$\begin{aligned} \mathcal{FHN}(\mathcal{T}) := \{ &\mathbf{M} \in \mathbb{H}(\mathbf{div} \mathbf{div}, \Omega); \mathbf{n} \cdot \mathbf{M}\mathbf{n}|_E \in \mathcal{P}^0(E), \mathbf{n} \cdot \mathbf{div} \mathbf{M} + \partial_t(\mathbf{t} \cdot \mathbf{M}\mathbf{n})|_E \in \mathcal{P}^0(E), \\ &\text{for all edges } E \text{ of the triangulation } \mathcal{T}\}. \end{aligned}$$

For details on the construction of this space (more precisely its trace space) and its approximation properties, we refer to [24, Section 6]. Finally we set  $\widehat{\mathfrak{U}}_{hk}$  to be the image of the trace operator  $\text{tr}^{\text{sK}}$  acting on

$$[\mathcal{P}^{k+1}(\mathcal{T}) \cap H^1(\Omega)]^2 \times \mathcal{HCT}(\mathcal{T}) \times [\mathcal{RT}^0(\mathcal{T})]^2 \times \mathcal{FHN}(\mathcal{T}),$$

and use the approximation spaces

$$\mathfrak{U}_{a,hk} := ([\mathcal{P}^0(\mathcal{T})]^2 \times \mathcal{P}^0(\mathcal{T}) \times [\mathcal{P}^0(\mathcal{T})]^{2 \times 2} \times [\mathcal{P}^0(\mathcal{T})]^{2 \times 2} \times \widehat{\mathfrak{U}}_{hk}) \cap \mathfrak{U}_a, \quad k = 0, 1.$$

Here, the parameter  $a$  refers to the type of boundary condition. Previously we used  $a \in \{c, s\}$  for the clamped and simply supported cases. Now, this notation generically refers to the space satisfying the required boundary conditions. Considering an ultraweak formulation, we treat all boundary conditions like essential ones. In the examples below, we only describe the kinematic constraints (i.e., boundary conditions for the primal variables  $w, \mathbf{u}$ ). The remaining conditions

for  $\mathbf{N}$  and  $\mathbf{M}$ , which are dual to the ones for  $\mathbf{u}$  and  $w$ , respectively, are taken to be homogeneous. We also stress the fact that the only difference between the cases  $k = 0$  and  $k = 1$  consists in the increased polynomial degree for the trace of the tangential displacements. This specific enrichment aims at alleviating the membrane locking effect.

Membrane locking is caused by the fact that the discrete approximation space for the displacements cannot produce bending modes with vanishing membrane strains. Depending on the exact nature of the bending mode, some or all components of the membrane strain tensor shall vanish. The former happens, e.g., for the various boundary and interior layer modes whereas the latter case is possible if the kinematic constraints are sufficiently weak to allow pure bending, or isometric transformations of the middle surface. Even though the locking mechanism for the DPG method may not be identical to that of standard displacement based finite elements, we expect that increasing the approximation degree of the trace variables associated with the tangential displacements shall alleviate the locking effect. Indeed, this is what we observe in the examples below.

**Remark 10.** *Static condensation of the field approximation variables is possible, and would drastically reduce the overall degrees of freedom to the ones associated with the trace variables. We do not consider this elimination of field variables in our experiments.*

*Furthermore, instead of using general (non-symmetric) approximations of  $\mathbf{N}$  as we do, one can consider symmetric discretizations. This change eliminates the test variable  $\mathbf{Q}$  because  $(\mathbf{N}, \mathbf{Q}) = 0$  for any  $\mathbf{Q} \in \mathbb{L}_2^k(\mathcal{T})$  is then satisfied automatically and since the trace operator is independent of  $\mathbf{Q}$ , cf. (8).*

For the discretization of the test space we use

$$\mathfrak{V}_h := \mathfrak{V}_h(\mathcal{T}) := [\mathcal{P}^3(\mathcal{T})]^2 \times \mathcal{P}^3(\mathcal{T}) \times [\mathcal{P}^3(\mathcal{T})]^{2 \times 2, \text{sym}} \times [\mathcal{P}^4(\mathcal{T})]^{2 \times 2, \text{sym}} \times [\mathcal{P}^2(\mathcal{T})]^{2 \times 2, \text{skew}}$$

where the notation “sym” and “skew” in the upper indices refers to the subsets of symmetric and skew-symmetric tensors, respectively. The choices of polynomial degrees for the first four components are based on the constructions in [26, 22] where Fortin operators are provided for a linear elasticity problem and a Kirchhoff–Love plate bending model. They use the same discretization spaces for the field and trace variables. Though, in our case, the construction of Fortin operators that are uniformly bounded in  $d$  is an open problem. This is due to the parameter-dependent coupling of terms in the norm of the test space, cf. (6). However, our numerical examples below indicate that our choice is reasonable.

Let

$$\eta^2 := \sum_{T \in \mathcal{T}} \eta(T)^2 := \sum_{T \in \mathcal{T}} \|B\mathbf{u}_h - L\|_{\mathfrak{V}_h(T)'}^2 = \|B\mathbf{u}_h - L\|_{\mathfrak{V}_h(\mathcal{T})'}^2 \quad (34)$$

denote the DPG built-in error estimator which—provided the existence of a Fortin operator—is reliable and efficient up to an oscillation term, see [9]. Here,  $\mathbf{u}_h \in \mathfrak{U}_{a,hk}$  is the DPG approximation and  $\mathfrak{V}_h(T)$  denotes the discrete test space on one element. We use this estimator to steer adaptive mesh refinements, marking elements for refinement by the bulk criterion

$$\theta \eta^2 \leq \sum_{T \in \mathcal{M}} \eta(T)^2.$$

Here,  $\mathcal{M} \subset \mathcal{T}$  is a set of minimal cardinality and we choose  $\theta = 1/4$ . The newest-vertex bisection rule is used to divide each marked element  $T \in \mathcal{M}$  into four triangles of equal area. We refer to uniform refinement when each element is marked for refinement, i.e.,  $\mathcal{M} = \mathcal{T}$ .

In the following, let  $\mathbf{u} = (\mathbf{u}, w, \mathbf{N}, \mathbf{M}, \widehat{\mathbf{u}})$  and  $\mathbf{u}_h = (\mathbf{u}_h, w_h, \mathbf{N}_h, \mathbf{M}_h, \widehat{\mathbf{u}}_h) \in \mathfrak{U}_{a,hk}$  be the generic exact solution and its DPG approximation, respectively. We denote  $\mathbf{u} = (u_1, u_2)$  and  $\mathbf{N} = (N_{ij})$ , and use the following abbreviations in the presentation of numerical results,

$$\begin{aligned} \text{err}(w_h) &:= d \|w - w_h\|, & \text{err}(\mathbf{u}_h) &:= \|\mathbf{C}_{\text{disp}}(\mathbf{u} - \mathbf{u}_h)\|, \\ \text{err}(\mathbf{M}_h) &:= d^{-1} \|\mathbf{M} - \mathbf{M}_h\|, & \text{err}(\mathbf{N}_h) &:= \|\mathbf{N} - \mathbf{N}_h\|, \end{aligned}$$

and  $\#\text{dof}$  is the dimension of  $\mathfrak{U}_{a,hk}$ . In the case of quasi-uniform meshes,  $\#\text{dof} = \mathcal{O}(h^{-2})$ . Note that, if  $\text{diam}(\Omega) \simeq D \simeq 1$ , then  $\text{err}(w_h) + \text{err}(\mathbf{u}_h) + \text{err}(\mathbf{M}_h) + \text{err}(\mathbf{N}_h) \lesssim \|\mathbf{u} - \mathbf{u}_h\|_{\mathfrak{U}}$ , cf. (13)

## 6.2 Scordelis–Lo cylindrical shell roof

Adopting the measurement units from [28], the Scordelis–Lo benchmark problem can be formulated by choosing

$$\Omega = (0, R) \times (0, \alpha R), \quad \mathbf{B} = \begin{pmatrix} 0 & 0 \\ 0 & 1/R \end{pmatrix} \quad \text{with} \quad R = 25, \quad \alpha = 2\pi/9,$$

corresponding to a quarter of the full roof, cut at  $x = 0$  and  $y = 0$ . Recalling the employed scaling of the displacements, the forcing corresponding to a uniformly distributed vertical load  $g$  is defined as

$$\mathbf{p} = (p_1, p_2), \quad p_1 = 0, \quad p_2 = \frac{g}{dE} \sin\left(\frac{y}{R}\right), \quad f = -\frac{g}{dE} \cos\left(\frac{y}{R}\right).$$

The symmetry boundary conditions at the cut lines are

$$u_1|_{x=0} = 0, \quad \partial_{\mathbf{n}} w|_{x=0} = 0, \quad u_2|_{y=0} = 0, \quad \partial_{\mathbf{n}} w|_{y=0} = 0,$$

and the conditions of the rigid diaphragm at the end of the roof are

$$u_2|_{x=R} = 0, \quad w|_{x=R} = 0.$$

For the values

$$E = 4.32 \cdot 10^8, \quad g = 90, \quad \nu = 0, \quad d = 0.25,$$

the vertical displacement at the midpoint of the free edge is evaluated as

$$u_2(0, \alpha R) \sin \alpha - w(0, \alpha R) \cos \alpha \approx 0.3086. \tag{35}$$

For this problem, a stronger tensor  $\mathbf{C}_{\text{disp}}$  than specified in (33) can be taken. Indeed, by the form of  $\mathbf{B}$  (vanishing curvature in  $x$ -direction) and the boundary condition  $v_1|_{x=0} = 0$  (implied

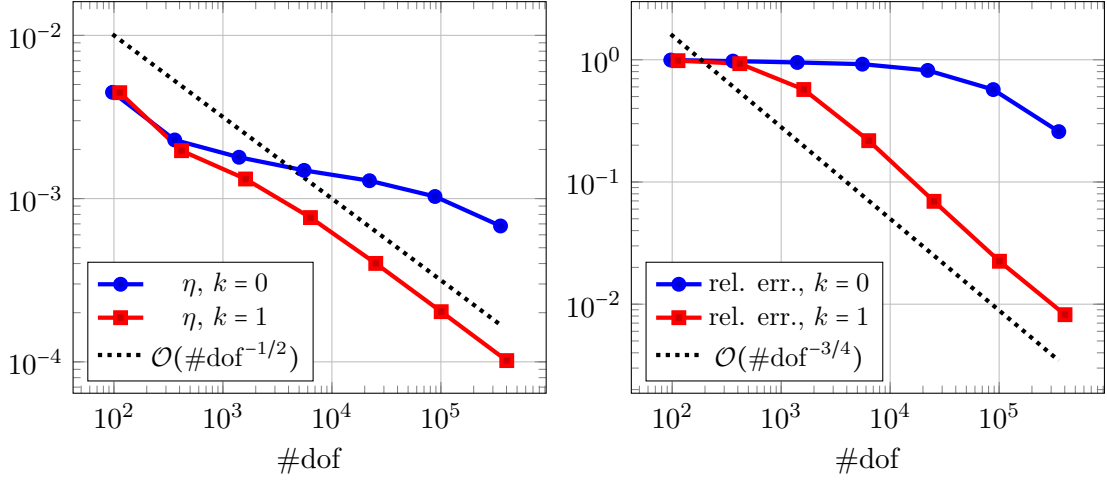


Figure 1: Scordelis–Lo. Left: error estimator  $\eta$ , right: errors for reference value (35).

by the one for  $u_1$ ) where  $\mathbf{v} = (v_1, v_2)$ , Poincaré–Friedrichs inequality yields  $\|v_1\| \leq R\|\partial_x v_1\| \leq R\|\boldsymbol{\varepsilon}\mathbf{v} - \mathbf{B}z\|$ . The  $v_2$ -component is controlled as in (33). Therefore, (15) holds with  $D = R$  and  $\mathbf{C}_{\text{disp}} = \text{diag}(1, d/R)$ , our selection for this example.

The following results are obtained with uniform mesh refinements. The left plot in Figure 1 compares the error estimators  $\eta$  provided by the DPG framework, cf. (34). We observe a moderate locking effect when using the space  $\mathfrak{U}_{a,h0}$  which is alleviated when switching to  $\mathfrak{U}_{a,h1}$ . The right plot compares the relative errors for the approximation of the vertical displacement (35). As expected we obtain better results when using  $\mathfrak{U}_{a,h1}$ . In fact, in the case  $k = 1$ , we observe a convergence with rate  $\mathcal{O}(\#\text{dof}^{-3/4}) = \mathcal{O}(h^{3/2})$  after only a brief pre-asymptotic behavior. We note that the discrete value is computed using the piecewise constant approximations to  $w$  and  $\mathbf{u}$  in (35).

An important feature of our method is its ability to approximate stress resultants robustly even on relatively coarse meshes. This is demonstrated in Figure 2 showing the distribution of the in-plane shear force approximation of  $N_{12}$  on different meshes. This quantity of interest is known to be rather difficult to approximate for some shell finite element formulations, see, e.g., [1].

### 6.3 Pitkäranta cylindrical shell obstacle course

For this set of problems we choose

$$\Omega = (-1, 1) \times (0, \pi/4), \quad \mathbf{B} = \begin{pmatrix} 0 & 0 \\ 0 & 1 \end{pmatrix}, \quad E = 1, \quad \nu = 0, \quad f(x, y) = \cos(2y)$$

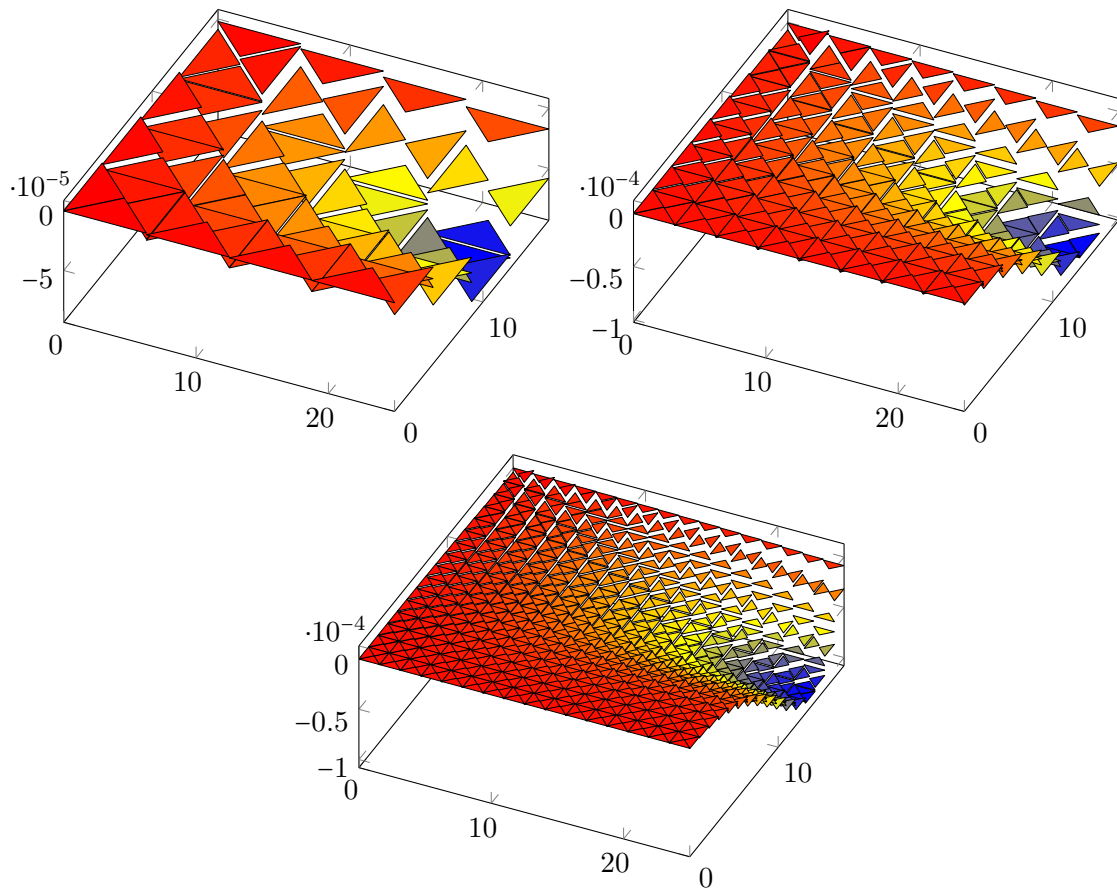


Figure 2: Scordelis-Lo, approximation of  $N_{12}$ ,  $k = 1$ . Meshes with 64, 256, 1024 elements.

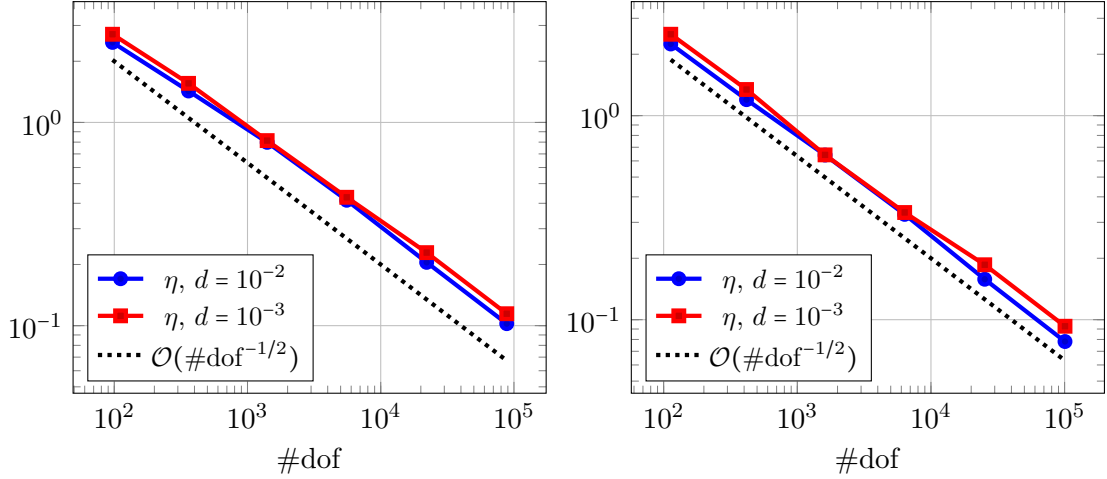


Figure 3: Clamped cylinder, error estimator  $\eta$ . Left:  $k = 0$ , right:  $k = 1$ .

and throughout the boundary conditions

$$w|_{y=\pi/4} = 0, \quad \partial_{\mathbf{n}} w|_{y=0} = 0, \quad u_1|_{y=\pi/4} = 0, \quad u_2|_{y=0} = 0. \quad (36)$$

They represent the symmetry of the problem on the full cylinder, restricted in our experiments to angles between 0 and  $\pi/4$ . Additional kinematic constraints will be specified for the individual cases, considered in the following subsections. Throughout we select the parameter  $D = 1$ .

### 6.3.1 Membrane state: cylinder with clamped ends

Additionally to (36), all displacements and the rotation are set to vanish along the curved ends,

$$w|_{x=\pm 1} = 0, \quad \partial_{\mathbf{n}} w|_{x=\pm 1} = 0, \quad \mathbf{u}|_{x=\pm 1} = 0.$$

By the arguments given previously in §6.2, and noting that  $\text{diam}(\Omega) \simeq 1$ , (15) is satisfied with our selection  $\mathbf{C}_{\text{disp}} = \text{diag}(1, d)$ . This case is membrane dominated and no relevant locking effect is expected. This is reflected by the results in Figure 3 which show the built-in error estimator for a sequence of uniform meshes. The values  $d = 10^{-2}, 10^{-3}$  are considered, on the left for  $k = 0$  and on the right for  $k = 1$ .

### 6.3.2 Inextensional state: cylinder with free ends

In this case we only impose the symmetry boundary conditions (36) and leave the curved ends free of kinematic constraints. This gives rise to the inextensional mode

$$w(x, y) = \frac{3}{4d^2} \cos 2y, \quad \mathbf{u} = -\frac{3}{8d^2} \begin{pmatrix} 0 \\ \sin 2y \end{pmatrix}$$

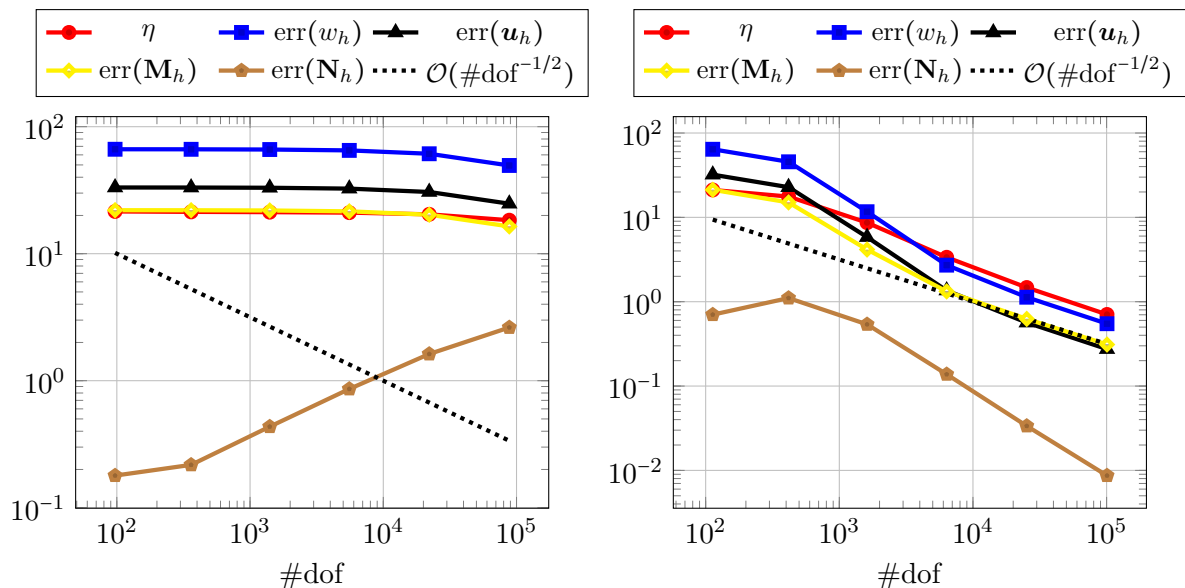


Figure 4: Free cylinder, errors and estimator  $\eta$ ,  $d = 10^{-2}$ . Left:  $k = 0$ , right:  $k = 1$ .

with vanishing membrane strains. Due to the lack of additional constraints we select  $\mathbf{C}_{\text{disp}} = \text{diag}(d, d)$ , as in (33). It is known that this example causes severe locking when using some standard finite element methods, cf. [42]. We consider uniform meshes. Figure 4 shows the errors and estimator for the moderate value  $d = 10^{-2}$ . We observe severe locking when using the space  $\mathfrak{U}_{a,hk}$  with  $k = 0$  (left plot). It is almost eliminated when increasing the polynomial degree for the approximation of the trace of the tangential displacements by one,  $k = 1$  (right plot). As expected, locking re-appears when considering smaller values of  $d$ . Figure 5 shows the results for  $d = 10^{-3}$  (left side) and  $d = 10^{-4}$  (right side), in both cases using the enriched trace space,  $k = 1$ . For  $d = 10^{-3}$  acceptable rates are observed after a pre-asymptotic phase whereas  $d = 10^{-4}$  causes severe locking.

### 6.3.3 Intermediate state: cylinder with simple sliding support at the ends

We impose boundary conditions (36) as before, and consider cylinder ends with simple sliding support,

$$w|_{x=\pm 1} = 0.$$

As in the case of free ends, the choice  $\mathbf{C}_{\text{disp}} = \text{diag}(d, d)$  implies that (15) holds. In this case the analytic expression of the solution is cumbersome. It can be computed reliably with computer algebra software that utilizes arbitrary-precision arithmetic. However, it is well known that for this problem boundary layers occur at  $x = \pm 1$ , cf. [42], and the effect of locking does not play

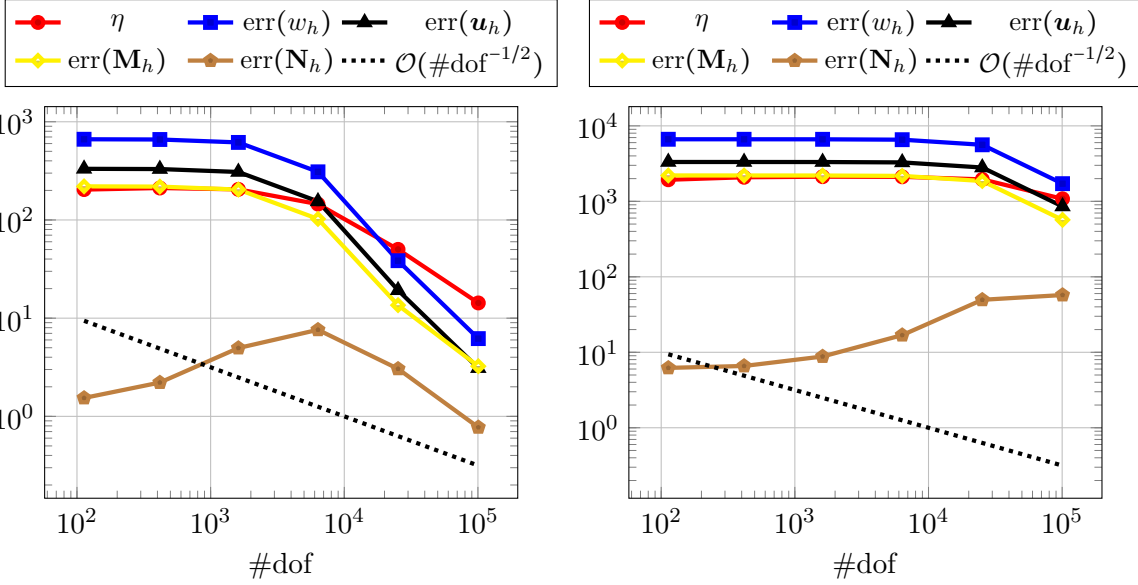


Figure 5: Free cylinder, errors and estimator  $\eta$ ,  $k = 1$ . Left:  $d = 10^{-3}$ , right:  $d = 10^{-4}$ .

an important role here. We consider  $d = 10^{-3}$  and compare the results for uniform and adaptive mesh refinements. In Figure 6 we present our results when using  $\mathfrak{U}_{a,h0}$  (the results for  $\mathfrak{U}_{a,h1}$  are basically the same and are not shown). They show that the adaptive variant nicely identifies the layer zones and reaches sooner the range of optimal convergence.

#### 6.4 Shallow shell subject to a concentrated load

We now consider shallow shells under a normal point load (delta distribution) at  $(0,0)$ , i.e.,  $f = \delta_{(0,0)}$  and  $\mathbf{p} = 0$ , cf. Remark 7. We study cases with elliptic, parabolic and hyperbolic middle surface:

$$\Omega = (-1, 1) \times (-1, 1), \quad \mathbf{B}_{\text{ell}} = \begin{pmatrix} 1 & 0 \\ 0 & 1 \end{pmatrix}, \quad \mathbf{B}_{\text{par}} = \begin{pmatrix} 0 & 0 \\ 0 & 1 \end{pmatrix}, \quad \mathbf{B}_{\text{hyp}} = \begin{pmatrix} 0 & 1 \\ 1 & 0 \end{pmatrix},$$

select  $E = 1$ ,  $\nu = 0$ ,  $D = 1$ , and consider  $d = 10^{-2}$  for all the examples in this subsection. For the actual computations we replace the delta distribution by a discrete version  $\delta_{h,(0,0)}$  which is supported on only one element  $T_0 \in \mathcal{T}$  such that  $(0,0)$  is a vertex of  $T_0$  and  $(\delta_{h,(0,0)}, z) = z|_{T_0}(0,0)$  for all  $z \in \mathcal{P}^3(\mathcal{T})$ .

For the elliptic and parabolic cases we impose the boundary conditions

$$w|_{\partial\Omega} = 0, \quad u_1|_{y=\pm 1} = 0, \quad u_2|_{x=\pm 1} = 0$$



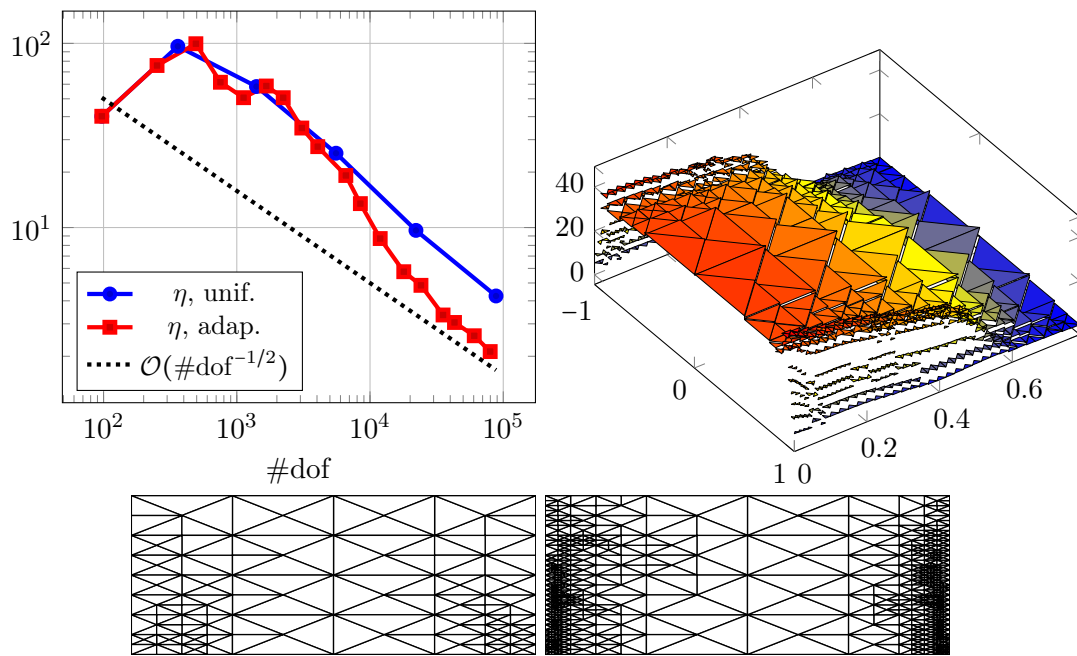


Figure 6: Cylinder with simple sliding support,  $d = 10^{-3}$ . Top left: error estimator  $\eta$  for uniform and adaptive refinements. Top right: transverse deflection  $w_h$  on adaptively refined mesh,  $\#\mathcal{T} = 1115$ . Bottom: adaptively refined meshes,  $\#\mathcal{T} = 186$  (left),  $\#\mathcal{T} = 1115$  (right). Equal axis scaling in bottom row.

corresponding to the expansions

$$\begin{aligned}
w(x, y) &= \sum_{m,n=1}^{\infty} W_{mn} \cos(m-1/2)\pi x \cos(n-1/2)\pi y, \\
u_1(x, y) &= \sum_{m,n=1}^{\infty} \alpha_{mn} \sin(m-1/2)\pi x \cos(n-1/2)\pi y, \\
u_2(x, y) &= \sum_{m,n=1}^{\infty} \beta_{mn} \cos(m-1/2)\pi x \sin(n-1/2)\pi y,
\end{aligned} \tag{37}$$

whereas for the hyperbolic case we impose

$$w|_{\partial\Omega} = 0, \quad u_1|_{x=\pm 1} = 0, \quad u_2|_{y=\pm 1} = 0$$

corresponding to

$$\begin{aligned}
w(x, y) &= \sum_{m,n=1}^{\infty} W_{mn} \cos(m-1/2)\pi x \cos(n-1/2)\pi y, \\
u_1(x, y) &= \sum_{m,n=1}^{\infty} \alpha_{mn} \cos(m-1/2)\pi x \sin(n-1/2)\pi y, \\
u_2(x, y) &= \sum_{m,n=1}^{\infty} \beta_{mn} \sin(m-1/2)\pi x \cos(n-1/2)\pi y.
\end{aligned} \tag{38}$$

#### 6.4.1 Elliptic case

In the elliptic case, the Fourier coefficients associated with (37) are

$$\begin{aligned}
W_{mn} &= \frac{12}{d^2(M^2 + N^2)^2 + 12}, \quad \alpha_{mn} = \frac{-12M}{d^2(M^2 + N^2)^3 + 12(M^2 + N^2)}, \\
\beta_{mn} &= \frac{-12N}{d^2(M^2 + N^2)^3 + 12(M^2 + N^2)} \quad \text{where } M := (m-1/2)\pi, \quad N := (n-1/2)\pi.
\end{aligned}$$

According to (33) we choose  $\mathbf{C}_{\text{disp}} = \text{diag}(d, d)$ . In Figure 7 we compare the errors for the field variables and the estimators for uniformly and adaptively refined meshes, in both cases using  $k = 0$ . For  $k = 1$  we get comparable results (not shown). We observe a rather long pre-asymptotic phase for the errors  $\text{err}(\mathbf{M}_h)$  and  $\text{err}(N_h)$  which is reduced by adaptivity. Figure 8 shows the solution  $N_{11}$  along the line  $y = 0$  together with its approximations ( $k = 0$ ) on the finest meshes of uniform and adaptive refinements. We observe that the maximum value of the approximation on the adaptive mesh provides a good approximation of the exact value.

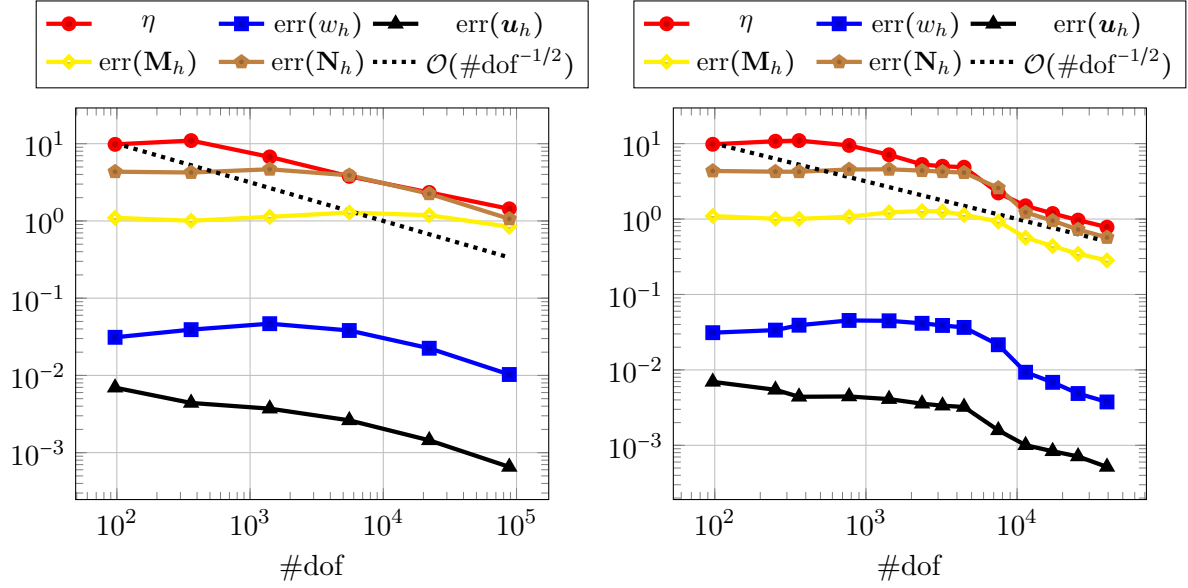


Figure 7: Elliptic shell with point load,  $d = 10^{-2}$ ,  $k = 0$ , errors and estimator  $\eta$ . Left: uniform meshes, right: adaptively refined meshes.

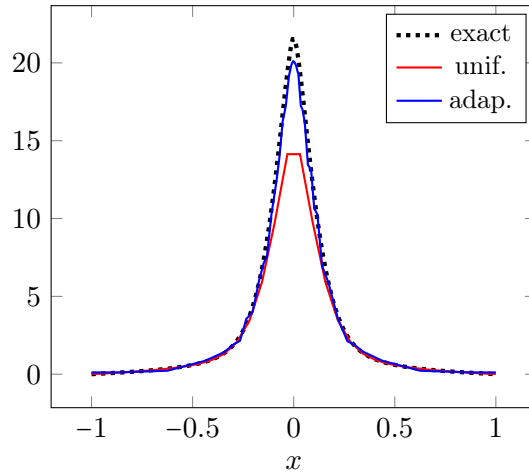


Figure 8: Elliptic shell with point load,  $d = 10^{-2}$ ,  $k = 0$ . Exact solution  $N_{11}$  along  $y = 0$  and its approximations with uniform mesh (4096 triangles) and adaptively refined mesh (1828 triangles).

### 6.4.2 Parabolic case

In the parabolic case, the Fourier coefficients associated with (37) are

$$\begin{aligned} W_{mn} &= \frac{12(M^2 + N^2)^2}{d^2(M^2 + N^2)^4 + 12M^4}, & \alpha_{mn} &= \frac{12MN^2}{d^2(M^2 + N^2)^4 + 12M^4}, \\ \beta_{mn} &= \frac{-24M^2N + 12N^3}{d^2(M^2 + N^2)^4 + 12M^4} & \text{where } M &:= (m - 1/2)\pi, N := (n - 1/2)\pi. \end{aligned}$$

As in the elliptic case we set  $\mathbf{C}_{\text{disp}} = \text{diag}(d, d)$ . In Figure 9 we compare the errors of the field variables and the estimator for uniform and adaptively refined meshes, in both cases for  $k = 0$  and  $k = 1$ . Contrary to the elliptic case, we observe stronger locking when using  $k = 0$ . In Figure 10 we compare the solution  $N_{22}$  along  $x = 0$  with its approximations on the finest uniform and adaptively refined meshes, using  $k = 1$ . Again, the adaptive version provides a good approximation of the maximum value of  $N_{22}$ .

### 6.4.3 Hyperbolic case

Finally, we consider the hyperbolic shell with point load. In this case, the Fourier coefficients associated with (38) are

$$\begin{aligned} W_{mn} &= \frac{12(M^2 + N^2)^2}{d^2(M^2 + N^2)^4 + 48M^2N^2}, & \alpha_{mn} &= \frac{-24N^3}{d^2(M^2 + N^2)^4 + 48M^2N^2}, \\ \beta_{mn} &= \frac{-24M^3}{d^2(M^2 + N^2)^4 + 48M^2N^2} & \text{where } M &:= (m - 1/2)\pi, N := (n - 1/2)\pi. \end{aligned}$$

By the structure of  $\mathbf{B}$  (vanishing diagonal) and the boundary conditions  $v_1|_{x=\pm 1} = v_2|_{y=\pm 1} = 0$  (corresponding to the conditions for  $\mathbf{u}$ ), we conclude that  $\|\mathbf{v}\| \leq 2\|\boldsymbol{\varepsilon}\mathbf{v} - \mathbf{B}\mathbf{z}\|$  so that (15) holds with  $\mathbf{C}_{\text{disp}} = \text{diag}(1, 1)$ . We select  $d = 10^{-2}$ , use the space  $\mathfrak{U}_{a,hk}$  with  $k = 1$ , and consider uniform and adaptive mesh refinements, as before with parameter  $\theta = 1/4$ . The DPG estimator  $\eta$  and errors are presented in Figure 11. We observe that, although the adaptive version does not necessarily lead to much smaller errors in all the variables, optimal rates for the field variables are seen for fewer degrees of freedom. Figure 12 shows two adaptively refined meshes. They show that the adaptive algorithm is able to localize distinctive features of the exact solution. In Figure 13 we compare an approximation  $w_h$  of the transverse deflection  $w$  generated by the adaptive algorithm (on the left) with the exact solution  $w$  (on the right). Here,  $w$  is calculated by cutting off its Fourier series after the first 10.000 terms ( $m, n = 1, \dots, 100$ ).

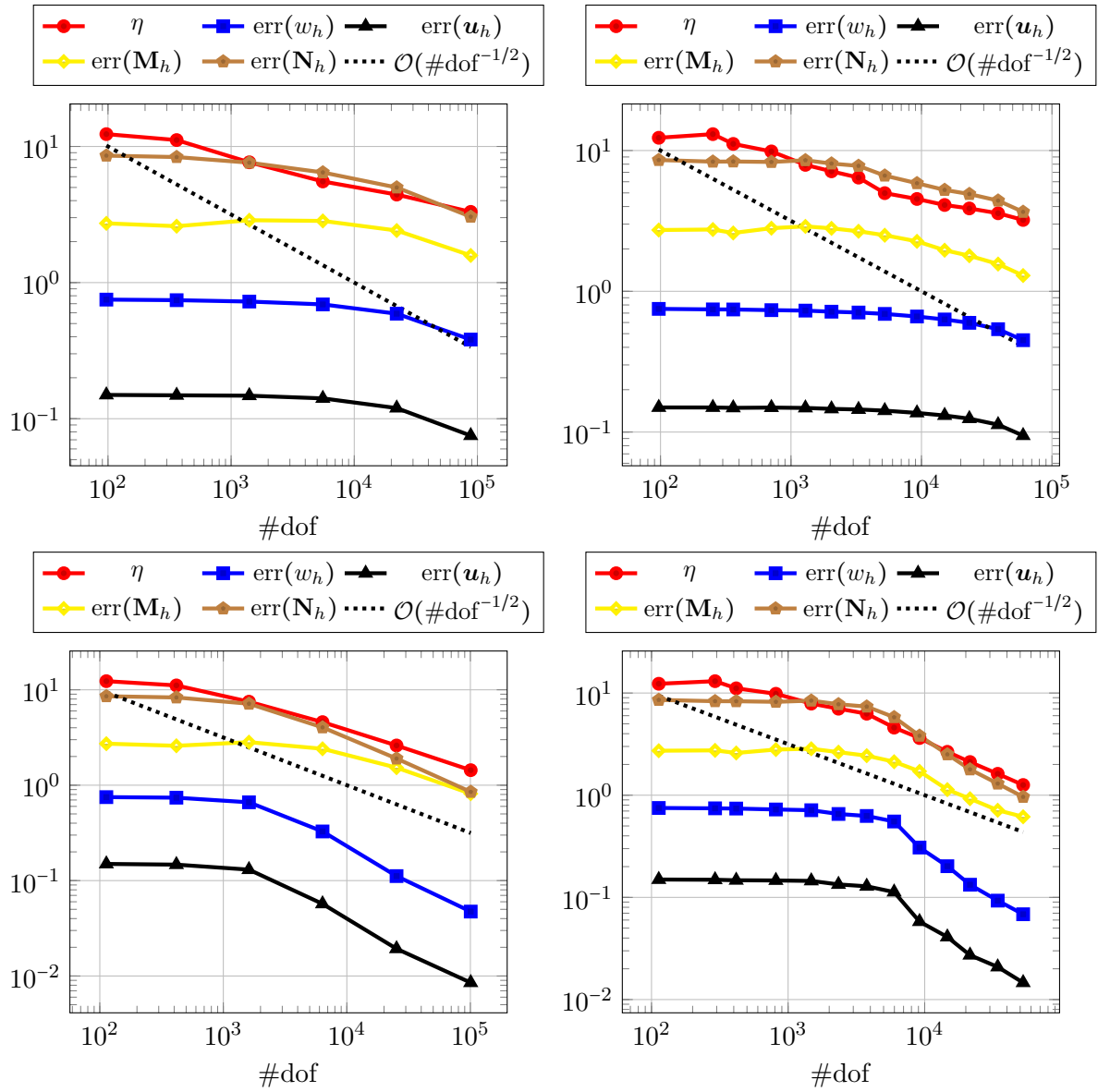


Figure 9: Parabolic shell with point load,  $d = 10^{-2}$ , errors and estimator  $\eta$ . Left: uniform meshes, right: adaptively refined meshes, top:  $k = 0$ , bottom:  $k = 1$ .

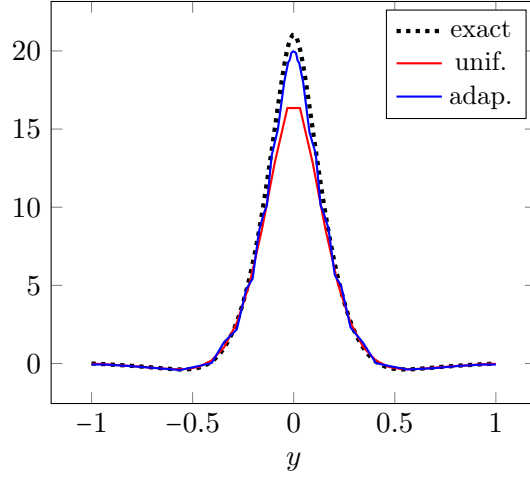


Figure 10: Parabolic shell with point load,  $d = 10^{-2}$ ,  $k = 1$ . Exact solution  $N_{22}$  along  $x = 0$  and its approximations with uniform mesh (4096 triangles) and adaptively refined mesh (2139 triangles).

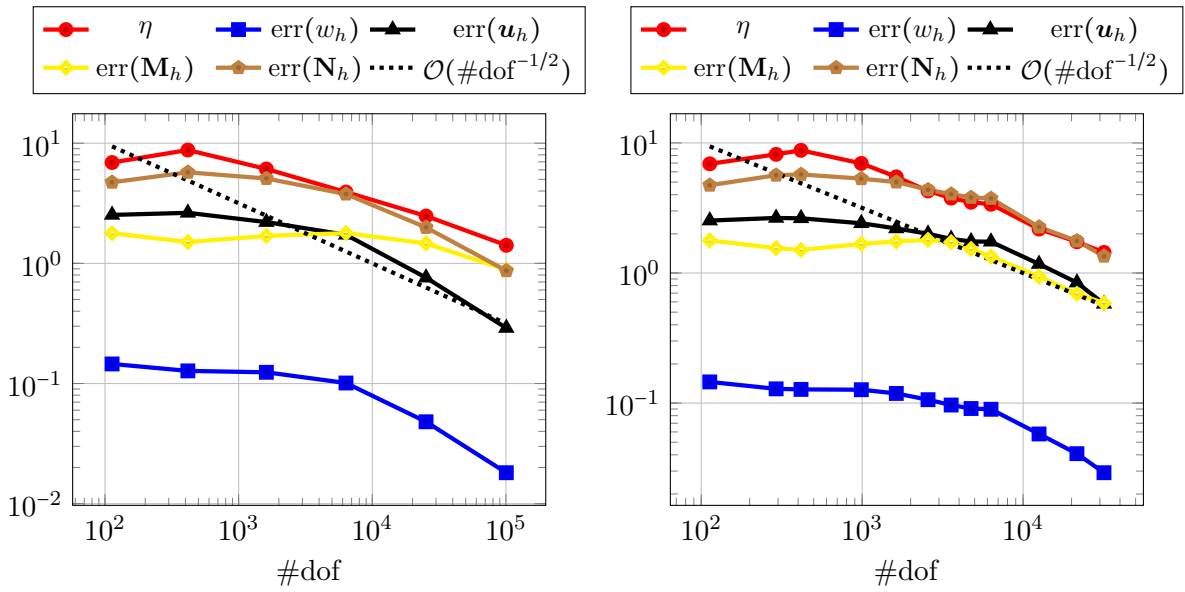


Figure 11: Hyperbolic shell with point load,  $d = 10^{-2}$ ,  $k = 1$ , errors and estimator  $\eta$ . Left: uniform meshes, right: adaptively refined meshes.

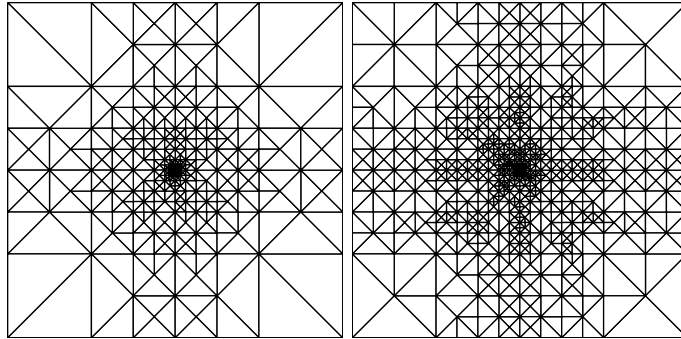


Figure 12: Hyperbolic shell with point load,  $d = 10^{-2}$ ,  $k = 1$ . Adaptively generated meshes, left: 510 triangles, right: 1294 triangles.

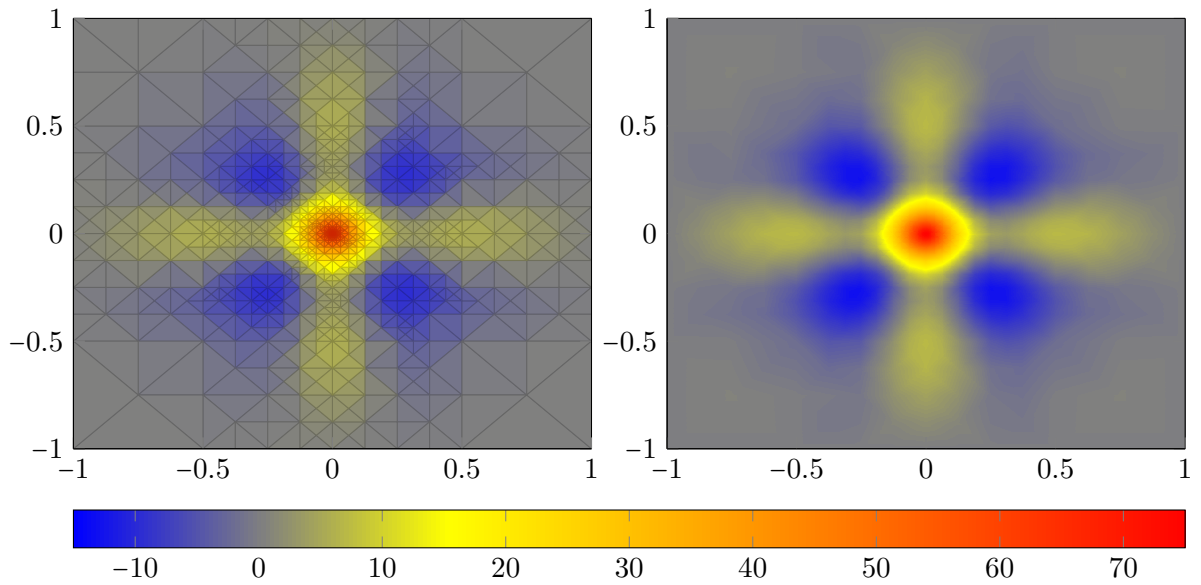


Figure 13: Hyperbolic shell with point load,  $d = 10^{-2}$ , transverse deflection. Left: approximation  $w_h$  on adaptively refined mesh ( $k = 1$ ), right: exact solution  $w$ .

## References

- [1] U. ANDEFINGER AND E. RAMM, *EAS-elements for two-dimensional, three-dimensional, plate and shell structures and their equivalence to HR-elements*, Internat. J. Numer. Methods Engrg., 36 (1993), pp. 1311–1337.
- [2] J. W. BARRETT AND K. W. MORTON, *Approximate symmetrization and Petrov-Galerkin methods for diffusion-convection problems*, Comput. Methods Appl. Mech. Engrg., 45 (1984), pp. 97–122.
- [3] F. BÉCHET, E. SANCHEZ-PALENCIA, AND O. MILLET, *Singularities in shell theory: anisotropic error estimates and numerical simulations*, Comput. Methods Appl. Mech. Engrg., 199 (2010), pp. 1326–1341.
- [4] J. BENZAKEN, J. A. EVANS, S. F. MCCORMICK, AND R. TAMSTORF, *Nitsche’s method for linear Kirchhoff–Love shells: formulation, error analysis, and verification*, Comput. Methods Appl. Mech. Engrg., 374 (2021), pp. 113544, 52.
- [5] C. L. BOTTASSO, S. MICHELETTI, AND R. SACCO, *The discontinuous Petrov-Galerkin method for elliptic problems*, Comput. Methods Appl. Mech. Engrg., 191 (2002), pp. 3391–3409.
- [6] J. BRAMWELL, L. F. DEMKOWICZ, J. GOPALAKRISHNAN, AND W. QIU, *A locking-free hp DPG method for linear elasticity with symmetric stresses*, Numer. Math., 122 (2012), pp. 671–707.
- [7] S. C. BRENNER AND L. R. SCOTT, *The Mathematical Theory of Finite Element Methods*, no. 15 in Texts in Applied Mathematics, Springer-Verlag, New York, 1994.
- [8] D. BRIASSOULIS, *Testing the asymptotic behaviour of shell elements—Part I: the classical benchmark tests*, Internat. J. Numer. Methods Engrg., 54 (2002), pp. 421–452.
- [9] C. CARSTENSEN, L. F. DEMKOWICZ, AND J. GOPALAKRISHNAN, *A posteriori error control for DPG methods*, SIAM J. Numer. Anal., 52 (2014), pp. 1335–1353.
- [10] ———, *Breaking spaces and forms for the DPG method and applications including Maxwell equations*, Comput. Math. Appl., 72 (2016), pp. 494–522.
- [11] O. CESSENAT AND B. DESPRÉS, *Application of an ultra weak variational formulation of elliptic PDEs to the two-dimensional Helmholtz problem*, SIAM J. Numer. Anal., 35 (1998), pp. 255–299.
- [12] D. CHAPELLE AND K. J. BATHE, *Fundamental considerations for the finite element analysis of shell structures*, Computers & Structures, 66 (1998), pp. 19–36.



- [13] L. F. DEMKOWICZ AND J. GOPALAKRISHNAN, *A class of discontinuous Petrov-Galerkin methods. Part I: the transport equation*, Comput. Methods Appl. Mech. Engrg., 199 (2010), pp. 1558–1572.
- [14] ———, *A class of discontinuous Petrov-Galerkin methods. Part II: Optimal test functions*, Numer. Methods Partial Differential Eq., 27 (2011), pp. 70–105.
- [15] ———, *An overview of the discontinuous Petrov Galerkin method*, in Recent developments in discontinuous Galerkin finite element methods for partial differential equations, vol. 157 of IMA Vol. Math. Appl., Springer, Cham, 2014, pp. 149–180.
- [16] L. F. DEMKOWICZ, J. GOPALAKRISHNAN, S. NAGARAJ, AND P. SEPÚLVEDA, *A spacetime DPG method for the Schrödinger equation*, SIAM J. Numer. Anal., 55 (2017), pp. 1740–1759.
- [17] L. F. DEMKOWICZ, J. GOPALAKRISHNAN, AND A. H. NIEMI, *A class of discontinuous Petrov-Galerkin methods. Part III: Adaptivity*, Appl. Numer. Math., 62 (2012), pp. 396–427.
- [18] L. F. DEMKOWICZ AND N. HEUER, *Robust DPG method for convection-dominated diffusion problems*, SIAM J. Numer. Anal., 51 (2013), pp. 2514–2537.
- [19] B. DESPRÉS, *Sur une formulation variationnelle de type ultra-faible*, C. R. Acad. Sci. Paris Sér. I Math., 318 (1994), pp. 939–944.
- [20] W. FLÜGGE, *Stresses in Shells*, Springer-Verlag, Berlin-Göttingen-Heidelberg, 1960. Translation of Statik und Dynamik der Schalen, Springer, 1934.
- [21] T. FÜHRER, A. HABERL, AND N. HEUER, *Trace operators of the bi-Laplacian and applications*, IMA J. Numer. Anal., 41 (2021), pp. 1031–1055.
- [22] T. FÜHRER AND N. HEUER, *Fully discrete DPG methods for the Kirchhoff–Love plate bending model*, Comput. Methods Appl. Mech. Engrg., 343 (2019), pp. 550–571.
- [23] ———, *A robust DPG method for large domains*, Comput. Math. Appl., 94 (2021), pp. 15–27.
- [24] T. FÜHRER, N. HEUER, AND A. H. NIEMI, *An ultraweak formulation of the Kirchhoff–Love plate bending model and DPG approximation*, Math. Comp., 88 (2019), pp. 1587–1619.
- [25] T. FÜHRER, N. HEUER, AND F.-J. SAYAS, *An ultraweak formulation of the Reissner–Mindlin plate bending model and DPG approximation*, Numer. Math., 145 (2020), pp. 313–344.
- [26] J. GOPALAKRISHNAN AND W. QIU, *An analysis of the practical DPG method*, Math. Comp., 83 (2014), pp. 537–552.
- [27] N. HEUER AND M. KARKULIK, *A robust DPG method for singularly perturbed reaction-diffusion problems*, SIAM J. Numer. Anal., 55 (2017), pp. 1218–1242.

- [28] R. H. MACNEAL, *Finite Elements: Their Design and Performance*, Marcel Dekker, Inc., 1994.
- [29] M. MALINEN, *On the classical shell model underlying bilinear degenerated shell finite elements*, *Internat. J. Numer. Methods Engrg.*, 52 (2001), pp. 389–416.
- [30] I. MERABET AND S. NICAISE, *A penalty method for a linear Koiter shell model*, *ESAIM Math. Model. Numer. Anal.*, 51 (2017), pp. 1783–1803.
- [31] A. H. NIEMI, *Approximation of shell layers using bilinear elements on anisotropically refined rectangular meshes*, *Comput. Methods Appl. Mech. Engrg.*, 197 (2008), pp. 3964–3975.
- [32] —, *A bilinear shell element based on a refined shallow shell model*, *Internat. J. Numer. Methods Engrg.*, 81 (2010), pp. 485–512.
- [33] —, *Benchmark computations of stresses in a spherical dome with shell finite elements*, *SIAM J. Sci. Comput.*, 38 (2016), pp. B440–B457.
- [34] A. H. NIEMI, H. HAKULA, AND J. PITKÄRANTA, *Point load on a shell*, in *Numerical Mathematics and Advanced Applications*, K. Kunisch, G. Of, and O. Steinbach, eds., Springer, Berlin, Heidelberg, 2008, pp. 819–826.
- [35] A. H. NIEMI, J. PITKÄRANTA, AND H. HAKULA, *Benchmark computations on point-loaded shallow shells: Fourier vs. FEM*, *Comput. Methods Appl. Mech. Engrg.*, 196 (2007), pp. 894–907.
- [36] J. PIILA, *Characterization of the membrane theory of a clamped shell. The elliptic case*, *Math. Models Methods Appl. Sci.*, 4 (1994), pp. 147–177.
- [37] —, *Characterization of the membrane theory of a clamped shell. The hyperbolic case*, *Math. Models Methods Appl. Sci.*, 6 (1996), pp. 169–194.
- [38] J. PIILA AND J. PITKÄRANTA, *Characterization of the membrane theory of a clamped shell. The parabolic case*, *Math. Models Methods Appl. Sci.*, 3 (1993), pp. 417–442.
- [39] —, *Energy estimates relating different linear elastic models of a thin cylindrical shell. I. The membrane-dominated case*, *SIAM J. Math. Anal.*, 24 (1993), pp. 1–22.
- [40] —, *Energy estimates relating different linear elastic models of a thin cylindrical shell. II. The case of free boundary*, *SIAM J. Math. Anal.*, 26 (1995), pp. 820–849.
- [41] J. PITKÄRANTA, *The problem of membrane locking in finite element analysis of cylindrical shells*, *Numer. Math.*, 61 (1992), pp. 523–542.
- [42] J. PITKÄRANTA, Y. LEINO, O. OVASKAINEN, AND J. PIILA, *Shell deformation states and the finite element method: a benchmark study of cylindrical shells*, *Comput. Methods Appl. Mech. Engrg.*, 128 (1995), pp. 81–121.

- [43] J. PITKÄRANTA, A.-M. MATAACHE, AND C. SCHWAB, *Fourier mode analysis of layers in shallow shell deformations*, *Comput. Methods Appl. Mech. Engrg.*, 190 (2001), pp. 2943–2975.
- [44] K. RAFETSEDER AND W. ZULEHNER, *A new mixed approach to Kirchhoff-Love shells*, *Comput. Methods Appl. Mech. Engrg.*, 346 (2019), pp. 440–455.
- [45] E. RAMM AND W. A. WALL, *Shell structures—a sensitive interrelation between physics and numerics*, *Internat. J. Numer. Methods Engrg.*, 60 (2004), pp. 381–427.
- [46] A. C. SCORDELIS AND K. S. LO, *Computer analysis of cylindrical shells*, *J. Am. Concr. Inst.*, 61 (1964), pp. 539–561.
- [47] S. ZHANG, *Analysis of a discontinuous Galerkin method for the bending problem of Koiter shell*, *Numer. Math.*, 133 (2016), pp. 333–370.